NASA TECHNICAL NOTE

NASA TN D-3697

c. 1

NASA TN D-3697

A SUMMARY OF LIGHT-INTENSITY DATA OF EIGHT TRAILBLAZER I REENTRY BODIES

by T. Dale Bess

Langley Research Center
Langley Station, Hampton, Va.

NATIONAL AERONAUTICS AND SPACE ADMINISTRATION • WASHINGTON, D. C. • NOVEMBER 1966

NASA TN D-3697

A SUMMARY OF LIGHT-INTENSITY DATA OF EIGHT TRAILBLAZER I REENTRY BODIES

By T. Dale Bess

Langley Research Center
Langley Station, Hampton, Va.

NATIONAL AERONAUTICS AND SPACE ADMINISTRATION

For sale by the Clearinghouse for Federal Scientific and Technical Information
Springfield, Virginia 22151 – Price $2.00

A SUMMARY OF LIGHT-INTENSITY DATA OF EIGHT TRAILBLAZER I REENTRY BODIES

By T. Dale Bess
Langley Research Center

SUMMARY

Results of experimental measurements of light intensity of the reentry test bodies of eight Trailblazer I vehicles are presented along with position and velocity measurements of each test body. In order to compare the luminous efficiencies of the eight Trailblazer I reentries with luminous efficiencies of higher velocity reentries, results of two high-velocity steel-pellet reentries are presented. All data were reduced from photographs taken with ballistic and modified aerial cameras located at various camera sites operated by NASA Langley Research Center. All flights were from Wallops Island, Virginia.

Tests were made on reentry bodies made of six different materials: aluminum, steel, copper, titanium, phenolic-nylon, and an epoxy-base material. The phenolic-nylon and the epoxy-base materials were ablative. Results of the light intensity measurements show that the amount of panchromatic light energy given off is largely due to the material of which the test object is made. The total integrated luminous energy of the metals in decreasing order were: titanium, steel, aluminum, and copper. The two reentries using phenolic-nylon and an epoxy-base material gave luminous intensities not nearly as bright as those of the metal reentries. The shape of the light curves of the ablative materials indicates that these materials have an almost constant intensity with no pronounced flaring. It is believed that flaring in some of the metal reentries represents fragmentation and burning through of the reentry body. Panchromatic luminous efficiencies are calculated for the eight Trailblazer I reentry test bodies. Comparing these luminous efficiencies with those of two high-velocity steel-pellet reentries shows that, in most instances, luminous efficiencies increase with increasing velocity. However, since the number of reentries for comparison purposes is not large enough, a dependence of luminous efficiency on velocity is difficult to establish.

INTRODUCTION

The advances in space technology in recent years have brought about a need for more basic research in many areas. One such area is the study of the physical phenomena which occur when high-speed objects reenter the earth's atmosphere. At the present time, much work is being done in this area. Some of the phenomena of high-speed reentry bodies have been simulated by using ground research facilities, but, in order to get a more complete understanding of the phenomena which occur at high-speed reentries, it becomes necessary to perform experimental, controlled reentries of test objects under real atmospheric conditions.

One such experiment, the Trailblazer I project, was designed to obtain controlled reentries in a real atmosphere. This experiment is accomplished by using a unique six-stage solid-fuel rocket designed to boost a test object to a desired altitude and have the object reenter the earth's atmosphere at hypersonic speeds. At sufficiently high reentry speeds, material dissociation and ionization of the atmospheric gases surrounding the body take place and cause a visible reentry of the test object.

The Trailblazer I project, which was essentially a materials study, was a cooperative effort with MIT Lincoln Laboratory to study the different physical phenomena occurring during visible reentry when test objects of different material, but with the same shape, reenter the earth's atmosphere at high speeds.

Basically, the two primary ways of monitoring the reentry object are multiple-frequency radar equipment and specialized ground-based photographic equipment. In order to use the photographic equipment effectively, the experiment must be carried out on a clear night during total darkness, and the reentry must occur as close as possible to the ground-based camera sites. The Trailblazer I vehicle was designed to obtain this desired reentry.

The radar equipment measured the radar signature of the reentry object as it is changed by the ionized atmosphere. The photographic equipment measured the radiated light energy from the reentry object when it is heated during reentry. Both photographic and radar equipment were also used to determine the velocity and the position in space of the reentry object.

The purpose of this paper is to present results of measurements of photographic data that have been reduced for eight Trailblazer I vehicles. Measurements of radiated light energy for the test body of each Trailblazer I flight are presented in graphical form. Velocity and position measurements for each reentry test body are summarized in tabular form.

SYMBOLS

d	distance along reentry trail, kilometers
h	altitude of reentry, kilometers

I	power, watts
M_p	absolute panchromatic magnitude
M'	uncorrected magnitude
ΔM_V	"writing-speed" correction for magnitude
ΔM_R	range correction for magnitude
ΔM_Z	atmospheric-absorption correction for magnitude
ΔM_t	correction to magnitude for cameras with occulting shutter
ΔM_r	magnitude correction due to reciprocity failure of film emulsion
Δm	mass loss during panchromatic reentry, grams
R	slant range of reentry from observation sites, kilometers
t	time, seconds
V	velocity of reentry, kilometers/second
ρ	air density, kilograms/meter^3
ρ_o	air density at sea level, kilograms/meter^3
τ	luminous efficiency
τ_p	panchromatic luminous efficiency
τ_o	luminosity coefficient, seconds/kilometer
δ	effective heat of ablation, joules/kilogram

Subscripts:

b	beginning
m	middle
e	end

DESCRIPTION OF EXPERIMENT

The injection into the earth's atmosphere of a high-speed test object was accomplished by using the six-stage Trailblazer I rocket vehicle shown in figure 1 and described in reference 1. The Trailblazer concept is unique in that the first three stages place a spin-stabilized velocity package outside the earth's atmosphere and the remaining stages, housed within the velocity package, are pointed backward toward the launch site so that reentry will occur close to multiple-stationed radar and photographic equipment. Figure 2 shows a plot of the nominal variation of altitude with horizontal range of the Trailblazer I vehicle from launch until reentry. The upper and lower limits of visible reentry are indicated. The sixth stage is the test object. This stage is a 12.7-centimeter-diameter spherical rocket motor known as the Cygnus 5 which attains the final reentry velocity. Trailblazer Ik and Trailblazer Im vehicles had 20.32-centimeter-diameter spheres mounted symmetrically around the Cygnus 5 motor. The increased weight of these reentry payloads resulted in a decrease in the reentry velocity. Figure 3 is a sketch of the velocity package. Figure 4 shows sketches of the reentry payloads for the eight Trailblazer I vehicles.

The panchromatic region of the reentry was photographed by both ballistic and modified aerial cameras with highly sensitive panchromatic film. BC-4 ballistic cameras and K-24 aerial cameras were the primary ones used in photographing the panchromatic reentry trail from the eight Trailblazer I reentry bodies. Some of the cameras, equipped with chopping shutters which opened and closed at known rates, produce a dashed image of reentry on the photographic plate. Data reduced from these plates give velocity and deceleration time histories of the visible reentry. Other cameras which operate without chopping shutters give a continuous reentry image on the photographic plate. The primary camera observation sites were located at Wallops Island, Virginia; Eastville, Virginia; and Coquina Beach, North Carolina. However, at different times, other observation sites were located at Langley Air Force Base, Virginia; Sandbridge, Virginia; and Fentress, Virginia. Photographs of the panchromatic region of the reentry trail of the eight Trailblazer I reentry bodies are shown in figure 5. The star background on the photographs appears as short streaks because of time exposures with stationary cameras.

Scratches are apparent on some of the photographs, particularly in the photographs of Trailblazers Ie and If. (See figs. 5(b) and (c), respectively.)

PROCEDURE

The procedure used to obtain velocity and position data follows closely that described in references 2 and 3. This procedure is a two-station method in which distances along the reentry trail from some arbitrary zero point are determined from the intersection of two planes, each of which is defined by the station coordinates, and the apparent reentry trail as seen from that station against a star background. For the region of interest, the reentry trail can be assumed to be a straight line. These distances along the reentry trail and their associated relative time, determined from shutter breaks along the trail, are fitted by the method of least squares to an equation of the form

$$d = a + bt + ce^{kt} \tag{1}$$

where a, b, c, and k are constants to be determined. Once the constants of this equation are established, the velocity and deceleration are determined by differentiation. The position coordinates in space of any point on the trail are also determined by the two intersecting planes.

The method of photometry applied in reducing all the Trailblazer I photographic data to obtain light curves is essentially the same as that used in natural meteor work. (See refs. 2 and 4.) The basic equations used and corrections applied are the same. The apparent stellar magnitude scale is used as a standard for comparison. In the method used to reduce Trailblazer data, the recording microdensitometer (a precision instrument designed to measure the percent of the light transmitted by a restricted area of an emulsion) is used to measure the variations in intensity along the reentry trail, whereas, in much of the natural meteor work, visual comparisons with known star magnitudes are employed. A calibration curve is obtained from microdensitometer traces of the star images. This curve is a plot of the density of star images against their stellar magnitudes. The magnitude of any point on the reentry trail is obtained by reading from the calibration curve the stellar magnitude which has the same density as the particular point on the reentry trail. Since errors in the calibration curve cause equal errors in the absolute magnitude of the reentry, a more thorough description of the calibration curve with its limitations is given in the appendix.

Before the absolute panchromatic magnitude of the panchromatic portion of the reentry trail can be obtained, there are some standard corrections to be made. A range correction and an atmospheric-absorption correction are necessary to normalize the reentry to 100 kilometers at zenith. The absorption correction used is that for a standard model atmosphere (ref. 5). The absorption correction does not take into account local atmospheric conditions such as haze. Any corrections due to these local conditions were minimized by requiring weather conditions that would give sixth magnitude stars at a 10° elevation through 7×10 binoculars. With these corrections, the magnitudes of points along the reentry trail are still in error in the sense that the much greater trailing velocity of the reentry body on the plate in millimeters per second relative to the trailing velocity of the stars has not been accounted for. This correction for the "writing speed" is the largest correction in magnitude. If all corrections are taken into account, the absolute panchromatic magnitude is expressed by the following equation (ref. 6):

$$M_p = M' + \Delta M_V + \Delta M_R + \Delta M_Z + \Delta M_t + \Delta M_r \tag{2}$$

In this equation, M' is the uncorrected magnitude; ΔM_V, the "writing speed" correction; ΔM_R, the range correction; and ΔM_Z, the atmospheric-absorption correction; ΔM_t represents a correction applied only to photographs taken with an occulting shutter and was zero for this report; ΔM_r represents a correction due to possible reciprocity failure of the film emulsion and was not included because the magnitude correction due to reciprocity failure is not known at the present time.

A relation obtained from the panchromatic magnitude of the reentry is the panchromatic luminous power of the reentry light expressed in watts. It is directly related to absolute panchromatic meteor magnitude by the following equation (ref. 6):

$$\log_{10} I = 2.90 - 4M_p \tag{3}$$

Equation (3) gives the power in watts whereas reference 6 has power expressed in ergs. Equation (3) differs slightly from the expression derived by Öpik in reference 7. The difference is due to the fact that Öpik's equation was derived by using the sensitivity curve of the human eye, whereas equation (3) was derived by using the sensitivity curve for panchromatic film. The difference is in the constant term and amounts to 0.20.

Equation (3) can be used for obtaining an intensity curve which is given as a plot of power in watts against either altitude or time along the panchromatic region of the reentry trail.

The total panchromatic luminous energy is obtained by integrating over the entire intensity curve. This luminous energy can be used to find a dimensionless panchromatic luminous efficiency factor τ_p which is defined as the fraction of kinetic energy converted into panchromatic radiation and is usually given as (ref. 8)

$$\tau_p = \frac{2}{\Delta m V^2} \int_{t_b}^{t_e} I dt \tag{4}$$

The limits of integration t_b and t_e are the beginning and end of panchromatic reentry; V is the velocity of the meteor and is assumed constant. The mass loss Δm is that fraction of the meteor that contributes to the reentry phenomena in the panchromatic region. For most natural meteors of small mass and velocities in excess of 10 km/sec,

τ_p is calculated on the assumption that all the mass of the meteor is consumed in producing the panchromatic trail. This is not true for the Trailblazer I reentries which were large bodies compared with most meteors and which reentered at velocities much lower than the slowest natural meteor. Thus, although the initial mass of the Trailblazer I reentry bodies was known, only a fraction of this mass may have been consumed in producing the reentry trail. To assume that the entire mass was consumed would lead to underestimates for the luminous efficiencies. Exactly how much mass is consumed during the panchromatic portion of the trail is difficult to calculate. However, if the heating rate over the reentry body is known and the effective heat of ablation of the material can be established, the approximate amount of material consumed in producing the panchromatic reentry trail can be calculated. One way to make the calculation is to divide the frontal area of the hemispherical reentry bodies into circular rings and integrate over each ring to find the mass loss contributed by each ring. Summing the mass loss of all the rings will give the total mass loss. The complete expression for the mass loss is

$$\Delta m = \frac{1}{\delta} \sum_{i=1}^{n} \sum_{j=1}^{m} \dot{q}_{ij} A_i \, \Delta t_j \tag{5}$$

Here δ is the effective heat of ablation of the material, A_i is the area of a particular circular ring, and Δt_j is the time increment at any altitude; $\dot{q}_{ij}$ is the laminar heating rate for a circular ring at any altitude (ref. 9).

In equation (5) all the quantities can be obtained with reasonable accuracy except the effective heat of ablation. The heat of ablation depends upon the type of ablation of the meteor material. Three types of ablation are considered: (1) vaporization at the surface which has the highest effective heat of ablation, (2) fusion of the material into molten drops which has a lower effective heat of ablation, and (3) fragmentation of the material in the solid state which has the lowest effective heat of ablation. For all the Trailblazer reentries, excluding the two using ablative material, ablation of the metal is possibly due to vaporization, fusion, and fragmentation. When this is the case, the effective heat of ablation is less than that for vaporization and greater than that for fragmentation. The heat of fusion of each of the metals is used for its effective heat of ablation in all calculations of mass loss. The two Trailblazer reentries using ablative material show no sign of fragmentation upon examining their light curves. Thus, the heat of ablation due to fragmentation is not considered. The ablative materials do not fuse into a liquid and therefore the heat of fusion is not considered. What does occur is that pyrolysis or sublimation of the material takes place and results in a higher effective heat of ablation than if fusion or fragmentation were the process. Table I gives the effective heats of ablation used for the six different materials.

These effective heats of ablation were taken from references 10 to 12. Once the amount of material ablated away by any reentry body is found, the panchromatic luminous efficiency τ_p follows directly from equation (4). The value of τ_p is small, usually less than 1 percent of the kinetic energy of the ablated mass. The calculated luminous efficiencies for each of the reentries are presented in table II.

That the luminous efficiency is, in general, proportional to some power of velocity is commonly accepted, and much work has been done in establishing this relation. Much of the work seems to favor a linear relation between τ and V. McCrosky in a report on simulated meteor reentry (ref. 13) assumed that luminous efficiency is proportional to the first power of velocity or

$$\tau = \tau_o V \tag{6}$$

where τ_o is a constant called the luminosity coefficient. Verniani in a report on the luminous efficiencies of meteors (ref. 14) shows that a power law $\tau = \tau_o V^n$ best represents τ as a function of velocity. The exponent n turns out to be 1.0 ± 0.15 for both faint and bright meteors. Thus, if this relation holds, the luminous efficiency τ should double when the velocity doubles, and so forth. Since the pellet reentries of Trailblazer Ig and Trailblazer IIb (refs. 15 and 6) have velocities about $1\frac{1}{2}$ to 2 times faster than any of the reentries discussed herein, their panchromatic luminous efficiencies are listed in table II for comparison purposes.

ACCURACY OF INTENSITY DATA

The intensity data for the reentry trails become inaccurate for very high and very low densities on the photographic image. The inaccuracies are due to the limitations of the film at these high and low densities. The film limitations are given by its characteristic curve; these limitations are also reflected in the calibration curve. A complete description of the calibration curve with its limitations is given in the appendix.

DISCUSSION OF RESULTS

Photographic data of the eight reentry trails are shown in figure 5. Differences in material, size, and weight of the reentry payloads caused the visible portion of the reentries to differ in velocity and position. For additional information, the position and velocity data reduced from photographic plates are presented in table III. These data represent the best-defined portion of the trail from which velocities can be computed and does not necessarily represent the entire panchromatic streak. Photographic data on Trailblazer Ij were insufficient for a velocity reduction. For this reason, the reentry velocity was obtained from radar data by matching altitudes from the optical reduction with radar altitudes. Agreement with expected velocity was good.

A brief description of the reentry payload for each vehicle is given in table IV along with a summary of the characteristics of the visible reentry. Six different materials were reentered: aluminum, copper, steel, titanium, phenolic-nylon, and epoxy-base material. The light curves for these reentries are presented in figure 6. Panchromatic magnitude is plotted against both altitude and time along the reentry trail. For those reentries which do not have position and velocity reduction for a portion of the panchromatic trail, as a result of poorly defined chops on the reentry streak, the chopped photographs were extrapolated to higher and lower altitudes in order to include the entire panchromatic region of reentry shown on the streak photographs. This extrapolation presents no problem since measured distance along the photographic image of reentry bears a linear relation with altitude.

Figure 7 is a plot of the power in watts against altitude for the eight reentries. This figure shows that the two aluminum reentries peaked at about the same altitude, 43.5 kilometers. There is strong evidence that this peak intensity represents fragmentation or burning through of the reentry body. This is supported by the fact that one of the aluminum reentry bodies, lined with a salt-saturated foam, had strong sodium lines at an altitude of 43.5 kilometers, the same altitude where major flaring occurred (ref. 16). The titanium reentry had its peak intensity at an altitude of about 42 kilometers and again at 37.5 kilometers where the titanium reentry body appears to have broken up. One steel reentry had its peak intensity at an altitude of about 40.5 kilometers and the other at about 44 kilometers. The reentry body with the thin copper shield became luminous at an altitude of 54 or 55 kilometers; its light curve had two peaks of about the same magnitude. The dip in the light curve between the two peaks possibly represents the altitude at which the thin copper shield burned through to the aluminum case. Light curves of the ablative material reentries had almost constant luminous intensities over the entire panchromatic trail. One of the ablative reentry bodies had a cesium-saturated plastic foam underneath the ablative material, but there was no evidence from photographs of reentry that the ablative material burned through to the cesium. This fact, together with the absence of flaring, indicates that the ablative materials did not burn through during the panchromatic region of reentry and possibly survived until impact.

Figure 8 is a graph of the average power in watts and the lifetime of the panchromatic reentries in seconds. The total energy in joules for each reentry is the area under the respective curves. The total integrated luminous energy of the reentries are easily obtained from this figure. The metals in order of decreasing total integrated luminous energy produced were: titanium, steel, aluminum, and copper. For the two ablative materials, phenolic-nylon had a greater total integrated luminous energy.

For these different materials of about the same mass and reentry velocity, the average power ranged from 260 to 37,000 watts. Thus, the intensity of the reentry trails depends strongly upon the material of the reentry body. The reentry trails of the ablative materials stay luminous for a longer time than the reentry trails of the metals because the mass of the ablative materials is not consumed as rapidly as the mass of the metals.

The calculated luminous efficiencies τ_p for the different reentries are presented in table II. These luminous efficiencies are a significant result of this report since they represent values of τ_p for reentry bodies at submeteoric velocities, whereas most of the data on luminous efficiencies of natural meteors are based on velocities in excess of 10 km/sec. It can be seen from table II that, with the exception of the Ic reentry, the luminous efficiencies for the eight Trailblazer I reentries are of the same order of magnitude. The Trailblazer Ic titanium reentry has a luminous efficiency of about an order of magnitude higher. The luminous efficiency for Ic could conceivably be an overestimate because of a characteristic of titanium in the atmosphere. It is the only known element which burns freely in nitrogen and it may therefore be that the effective heat of ablation is lower than the value used in calculating the ablated mass. A lower heat of ablation would lower the luminous efficiency. For the metallic materials, table II shows that titanium has the highest luminous efficiency, followed in decreasing order by steel, aluminum, and copper. For the two ablative materials phenolic-nylon has a luminous efficiency about twice as large as the epoxy-base material. Luminous efficiencies of two steel pellet reentries which had velocities of 9.8 km/sec and 11.9 km/sec, respectively, are included for comparison purposes to see the effect velocity can have on luminous efficiencies. In most cases, the two steel pellet reentries had greater luminous efficiencies than any of the Trailblazer I reentries regardless of the material of the reentry bodies. One exception was the titanium reentry which had a much higher luminous efficiency than either of the pellet reentries although its velocity was considerably less than either of the pellet reentry velocities. However, comparisons do not have much meaning unless the reentry bodies are made of the same material and the comparisons are therefore restricted to four reentries: the two pellet reentries, Trailblazer Ie reentry, and Trailblazer Ih reentry. Table II shows that the IIb pellet reentry, with its higher velocity, had the largest luminous efficiency. The Ig pellet reentry had a luminous efficiency greater than the Trailblazer Ih reentry but less than Trailblazer Ie reentry. Trailblazer Ie reentry had a luminous efficiency greater than either the Ig pellet reentry or the Trailblazer Ih reentry although its velocity was not as great. Results show that although luminous efficiency increases with velocity in most instances, there is one case in which it does not and until data from a larger number of reentries, utilizing the same material over a wide range of velocities are available, dependence of luminous efficiency on velocities will be difficult to determine. These results on luminous efficiencies point to the need for more research in determining a velocity dependence for luminous efficiencies. This research would require a number of reentries over a wide range of velocities where reentry bodies of different sizes, shapes, and materials could be tested.

CONCLUSIONS

Light curves obtained for six different materials which reentered the earth's atmosphere under similar conditions show that the amount of luminous energy given off and the shape of the light curve is largely dependent on whether the material is metallic or ablative. The ablative materials have panchromatic trails with low and almost constant intensity. They become visible at a greater altitude and stay visible longer than the visible trails of the metals. The panchromatic trails of the metal reentries have high intensities, short durations, and pronounced flaring. There is evidence that flaring represents fragmentation of the reentry body.

Panchromatic luminous efficiencies were obtained for the eight Trailblazer I reentries. Comparing their luminous efficiencies with the luminous efficiencies of two high-velocity steel-pellet reentries shows that luminous efficiency increases with increasing velocity in most instances. However, the number of comparisons was not sufficient to arrive at any dependence of luminous efficiency on increasing velocity. Results of this paper point to the need for more research in determining a velocity dependence for luminous efficiencies. This research would require a number of reentries over a wide range of velocities where reentry bodies of different sizes, shapes, and materials could be tested.

Langley Research Center,
National Aeronautics and Space Administration,
Langley Station, Hampton, Va., August 12, 1966,
709-06-00-01-23.

APPENDIX

THE CALIBRATION CURVE

A convenient way of estimating meteor magnitudes from photographs of meteor reentry is by comparing the meteor reentry image to line images of known star magnitudes. The line images result from stationary cameras with fixed exposure times. The comparison is made by means of a calibration curve. This curve is obtained by taking stars of known magnitude, preferably from around the reentry area, and plotting their stellar magnitude against film density. The density is a measure of the light transmission of the star images and is measured by a recording microdensitometer that scans across the line images. The density D is defined as

$$D = \log_{10} \frac{1}{T}$$

where T is the transmittance of light through the star images as measured by the recording microdensitometer.

A calibration curve is shown in figure 9(a). Stellar magnitude which is a logarithmic relation is plotted along the abscissa and density along the ordinate. It can be seen that this calibration curve is characterized by three distinct parts. It has a linear middle portion with its particular slope and the upper and lower ends with different slopes.

To obtain a calibration curve, a wide range of different magnitude stars are required, from the brighter stars to the dimmer stars preferably of the same color class. Experience has shown that the entire range can be covered by selecting 40 to 50 stars from around the reentry area of the reentry photograph. However, the upper end of the curve representing the higher densities is defined by using the brighter stars (less than third magnitude). This presents a problem because the number of stars in this magnitude range that have been cataloged is small. The lower end, representing the lower densities, is defined by using the dimmer stars (greater than eighth magnitude). There is an abundance of these dim stars, but many of the camera systems used to photograph the reentry are not fast enough to record many of the star images in the preferred color class. Also, the modern star charts used in identifying the stars as to type and magnitude do not list the very dim stars. The middle part of the curve which is usually referred to as the straight-line portion is more easily defined since it does not depend as much upon either the very bright or very dim stars for its definition. An improved calibration curve can be obtained by printing density step wedges on the reentry plates and using a few selected stars to assign magnitudes to the curve. Density step wedges were not printed on the eight Trailblazer I reentry photographic plates.

APPENDIX

The calibration curve is very similar to the characteristic H and D curve in photography which describes how a photographic material responds to exposure and development. However, the characteristic curve has log exposure of the material along the abscissa instead of stellar magnitudes as in the calibration curve. The form of the characteristic curve is shown in figure 9(b). It too has a straight-line portion where the density is linear with log exposure just as density varies linearly with stellar magnitude over a certain range of the calibration curve. The characteristic curve is also curved at each end, and the two ends of the curve are usually designated as the shoulder and toe of the curve.

Figure 9(b) is included to show similarity between the characteristic curve and the calibration curve. The slope of the straight-line part of the calibration curve is nearly the same as the slope of the characteristic curve. This is just a coincidence and is not generally true. The slope depends upon a number of factors such as the time of development and kind of photographic material being used.

Ordinarily, the calibration curve in figure 9(a) will show some scatter in the plot of stellar magnitudes against their density; but if enough points are plotted over the necessary magnitude range, there is still a trend showing the straight-line portion and the curved portions at each end. This being the case, the procedure is to break up the curve into three parts and fit each one to a straight line by the method of least squares. By fitting the upper and lower ends to a straight line, a good approximation to the exact calibration curve is obtained. The error in magnitude due to scatter is available for any density that is obtained from the calibration curve.

REFERENCES

1. Gardner, William N.; Brown, Clarence A., Jr.; Henning, Allen B.; Hook, W. Ray; Lundstrom, Reginald R.; and Ramsey, Ira W., Jr.: Description of Vehicle System and Flight Tests of Nine Trailblazer I Reentry Physics Research Vehicles. NASA TN D-2189, 1964.

2. Whipple, Fred L.; and Jacchia, Luigi G.: Reduction Methods for Photographic Meteor Trails. Smithsonian Contrib. Astrophys., vol. 1, no. 2, 1957, pp. 183-206.

3. Wilson, F. A.: Procedures and Computer Programs for Reduction of Ballistic Plates from Trailblazer I and II Programs. Technical Note 1965-8.

4. Jacchia, Luigi G.: Photographic Meteor Phenomena and Theory. Meteor Photometry, Fundamental Equations and Constants, Durations and Flares. Tech. Rept. No. 3, Harvard College Observatory and M.I.T., 1949.

5. Millman, Peter M.; and McKinley, D. W. R.: Meteor Echo Durations and Visual Magnitudes. Can. J. Phys., vol. 34, no. 1, Jan. 1956, pp. 50-61.

6. Ayers, Wendell G.: Luminous Efficiency of an Artificial Meteor at 11.9 Kilometers Per Second. NASA TN D-2931, 1965.

7. Öpik, Ernst J.: Physics of Meteor Flight in the Atmosphere. Interscience Publ., Inc., 1958, p. 147.

8. McKinley, D. W. R.: Meteor Science and Engineering. McGraw-Hill Book Co., Inc., 1961, p. 177.

9. Allen, H. Julian; and James, Nataline A.: Prospects for Obtaining Aerodynamic Heating Results From Analysis of Meteor Flight Data. NASA TN D-2069, 1964.

10. Hodgman, Charles D.; Weast, Robert C.; and Selby, Samuel M., eds.: Handbook of Chemistry and Physics. Thirty-seventh ed., Chemical Rubber Publ. Co., 1955-1956.

11. Gerasimov, Ya. I.; Krestovnikov, A. N.; and Shakhov, A. S.: Chemical Thermodynamics in Nonferrous Metallurgy. Vol. III. Thermodynamics of Tungsten, Molybdenum, Titanium, Zirconium, Niobium, Tantalum, and of Their More Important Compounds. NASA TT F-285 (TT 65-50 111), The Israel Program for Sci. Transl., 1965. (Available from c FSTI, U.S. Dept. Com.)

12. Darnell, Wayne L.: Radar Cross Section and Optical Radiation From the Trailblazer IIa 9° Half-Angle Blunt Nose Cone During Hypersonic Reentry. NASA TN D-3214, 1966.

13. McCrosky, Richard E.: Observation of Simulated Meteors. Smithsonian Contrib. Astrophys., vol. 5, no. 4, 1961, pp. 29-36.

14. Verniani, Franco: On the Luminous Efficiency of Meteors. Spec. Rept. No. 145, Smithsonian Inst. Astrophys. Obs., Feb. 17, 1964.

15. Jewell, W. O.; and Wineman, A. R.: Preliminary Analysis of a Simulated Meteor Reentry at 9.8 Kilometers Per Second. NASA TN D-2268, 1964.

16. Harvey, Gale A.: Photometric Analysis of Spectrograms of Two Trailblazer I Payload Reentry Events. NASA TN D-3389, 1966.

TABLE I. - EFFECTIVE HEATS OF ABLATION USED FOR SIX REENTRY MATERIALS

Material	Effective heat of ablation, δ, joules/kilogram
Titanium	1.55×10^6
Steel	1.31
Aluminum	.99
Copper	.63
Epoxy base	9.30
Phenolic-nylon	9.30

TABLE II. - CALCULATED LUMINOUS EFFICIENCIES

Vehicle designation	Material	Velocity, km/sec	Integrated energy, joules	Luminous efficiency, τ_p
Ic	Titanium	5.86	9.94×10^4	7.02×10^{-2}
Ie	Steel	5.42	8.20×10^3	8.26×10^{-3}
If	Copper	5.93	2.55	1.82
Ig	Steel pellet	9.80	6.50×10^2	7.6
Ih	Steel	6.36	1.05×10^4	5.04
Ii	Aluminum	5.93	3.80×10^3	2.57
Ij	Phenolic-nylon	6.28	5.43	9.37
Ik	Aluminum	5.57	7.92	2.12
Im	Epoxy base	5.16	1.37	4.60
IIb	Steel pellet	11.90	1.93	1.22×10^{-2}

TABLE III.- BALLISTICS DATA OF EIGHT TRAILBLAZER I REENTRY BODIES

Vehicle designation	Observation site	Time, sec	Slant range, km	Altitude, km	Velocity, km/sec
Ic	Coquina Beach, N.C.	t_b, 0.00 t_m, 1.20 t_e, 2.40	R_b, 114.44 R_m, 111.33 R_e, 108.82	h_b, 46.88 h_m, 40.28 h_e, 34.40	V_b, 5.87 V_m, 5.07 V_e, ---
Ie	Wallops Island, Va.	t_b, 0.00 t_m, 0.90 t_e, 2.35	R_b, 216.97 R_m, 215.78 R_e, 213.86	h_b, 44.85 h_m, 40.34 h_e, 34.62	V_b, 5.42 V_m, 4.60 V_e, ---
If	Fentress, Va.	t_b, 0.00 t_m, 0.77 t_e, 1.60	R_b, 200.09 R_m, 200.20 R_e, 200.42	h_b, 55.86 h_m, 52.18 h_e, 48.21	V_b, 5.72 V_m, 5.50 V_e, 5.34
Ih	Wallops Island, Va.	t_b, 0.00 t_m, 1.18 t_e, 2.74	R_b, 293.30 R_m, 294.10 R_e, 295.20	h_b, 53.27 h_m, 46.97 h_e, 39.77	V_b, 6.34 V_m, 5.83 V_e, 4.00
Ii	Coquina Beach, N.C.	t_b, 0.00 t_m, 0.75 t_e, 1.54	R_b, 125.21 R_m, 123.65 R_e, 122.19	h_b, 50.04 h_m, 45.74 h_e, 41.35	V_b, 5.97 V_m, 5.81 V_e, 4.71
Ij	Wallops Island, Va.	t_b, 0.00 t_m, 3.30 t_e, 7.00	R_b, 183.28 R_m, 169.76 R_e, 156.96	h_b, 70.00 h_m, 53.26 h_e, 36.05	V_b, 6.28 V_m, 5.98 V_e, 3.70
Ik	Coquina Beach, N.C.	t_b, 0.00 t_m, 1.69 t_e, 3.92	R_b, 116.95 R_m, 112.07 R_e, 107.44	h_b, 57.90 h_m, 48.95 h_e, 39.70	V_b, 5.57 V_m, 5.19 V_e, 3.32
Im	Sandbridge, Va.	t_b, 0.00 t_m, 2.65 t_e, 5.35	R_b, 173.40 R_m, 169.06 R_e, 165.80	h_b, 67.92 h_m, 55.17 h_e, 43.33	V_b, 5.16 V_m, 5.00 V_e, 4.27

TABLE IV. - CHARACTERISTICS OF REENTRY

Vehicle designation	Payload	Mass, kg	Reentry angle (measured from vertical), deg	Remarks
Ic	Heavy-wall Cygnus 5 titanium case	0.952	5.83	Prominent flare at 38.2 km; titanium appears to break up
Ie	Thick-wall Cygnus 5 steel case	1.040	13.52	Bright reentry; maximum intensity at 40.5 km
If	Thin-wall Cygnus 5 aluminum case with copper cap	0.903	27.69	Two maximums at 54.2 and 50.2 km; big dip between peaks
Ih	Thick-wall Cygnus 5 steel case	0.708	19.66	Maximum at 44 km; bright reentry
Ii	Thick-wall Cygnus 5 aluminum case	0.640	11.98	Bright reentry; maximum magnitude at 44 km
Ij	Cygnus 5 aluminum case with nylon cap	0.695	26.04	Very long and dim reentry; no flaring apparent
Ik	20.32-cm-diameter aluminum sphere; salt-impregnated plastic foam beneath sphere	1.180	11.79	Maximum intensity occurs at 43.5 km where aluminum case burned through
Im	20.32-cm-diameter epoxy-base sphere; cesium-saturated plastic foam beneath sphere	1.366	19.08	Very long and dim reentry; no apparent flares; no indication of case burning through

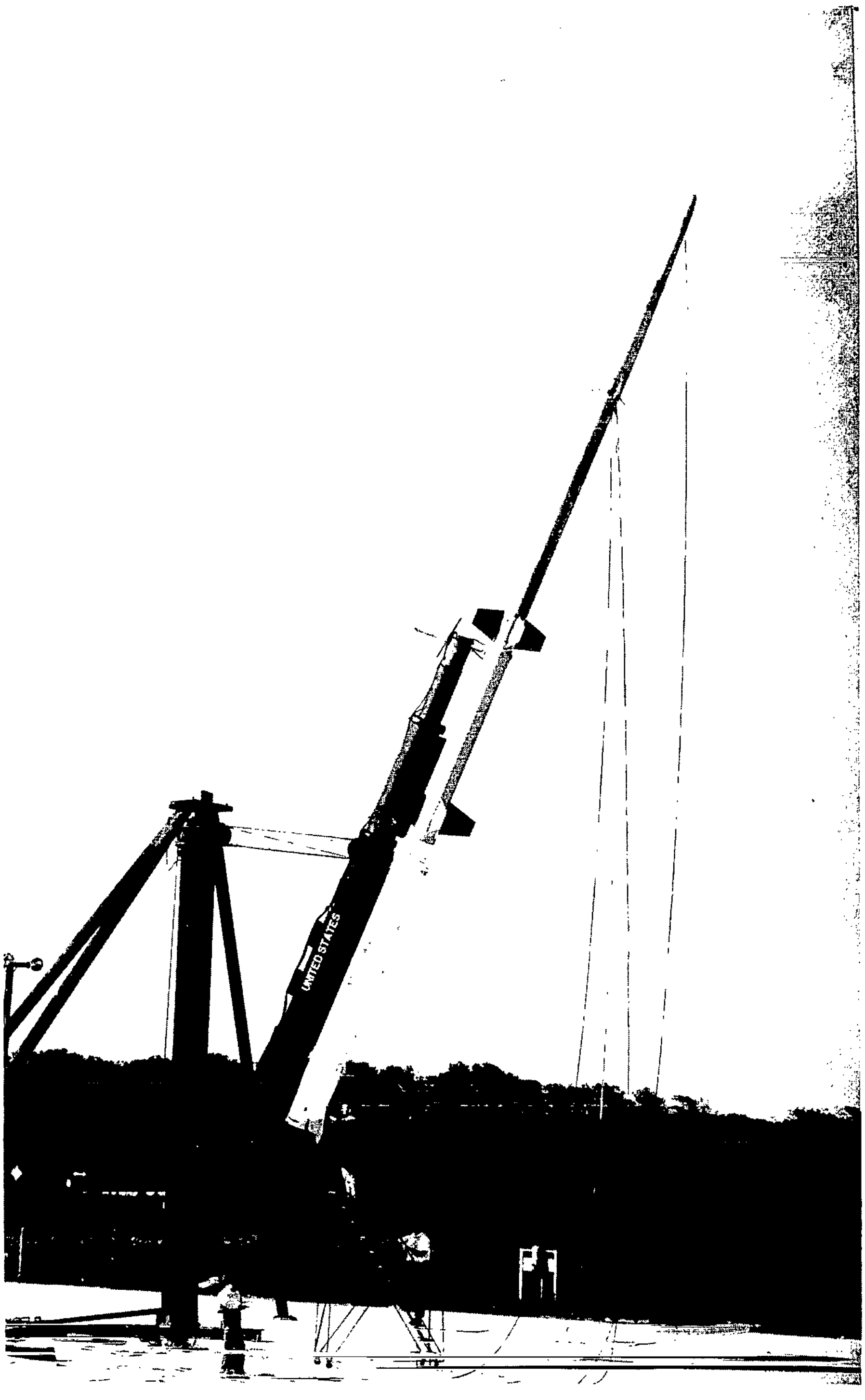

Figure 1.- Six-stage Trailblazer I on launch pad at Wallops Island, Va. L-61-5938

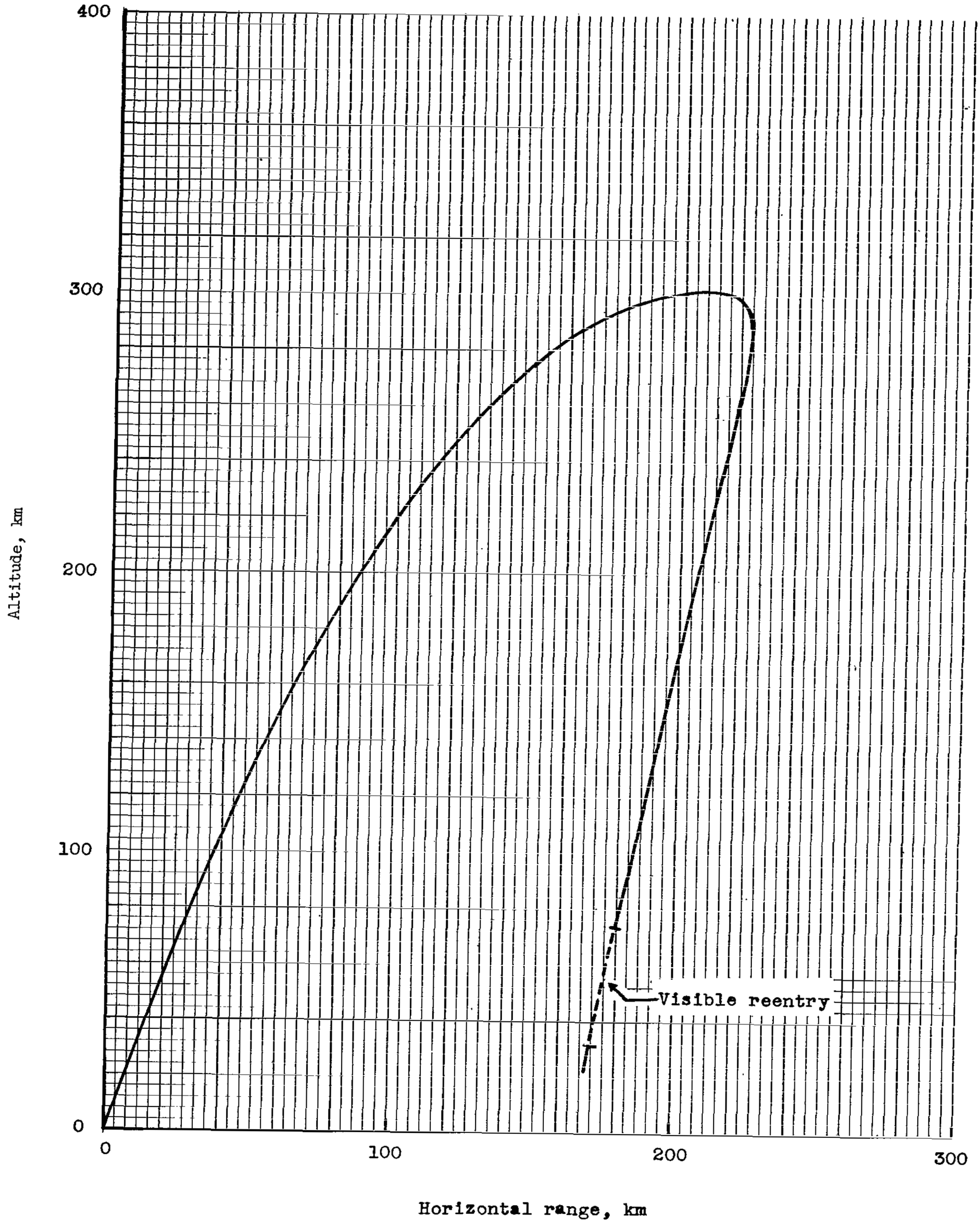

Figure 2.- Nominal trajectory of a Trailblazer I reentry.

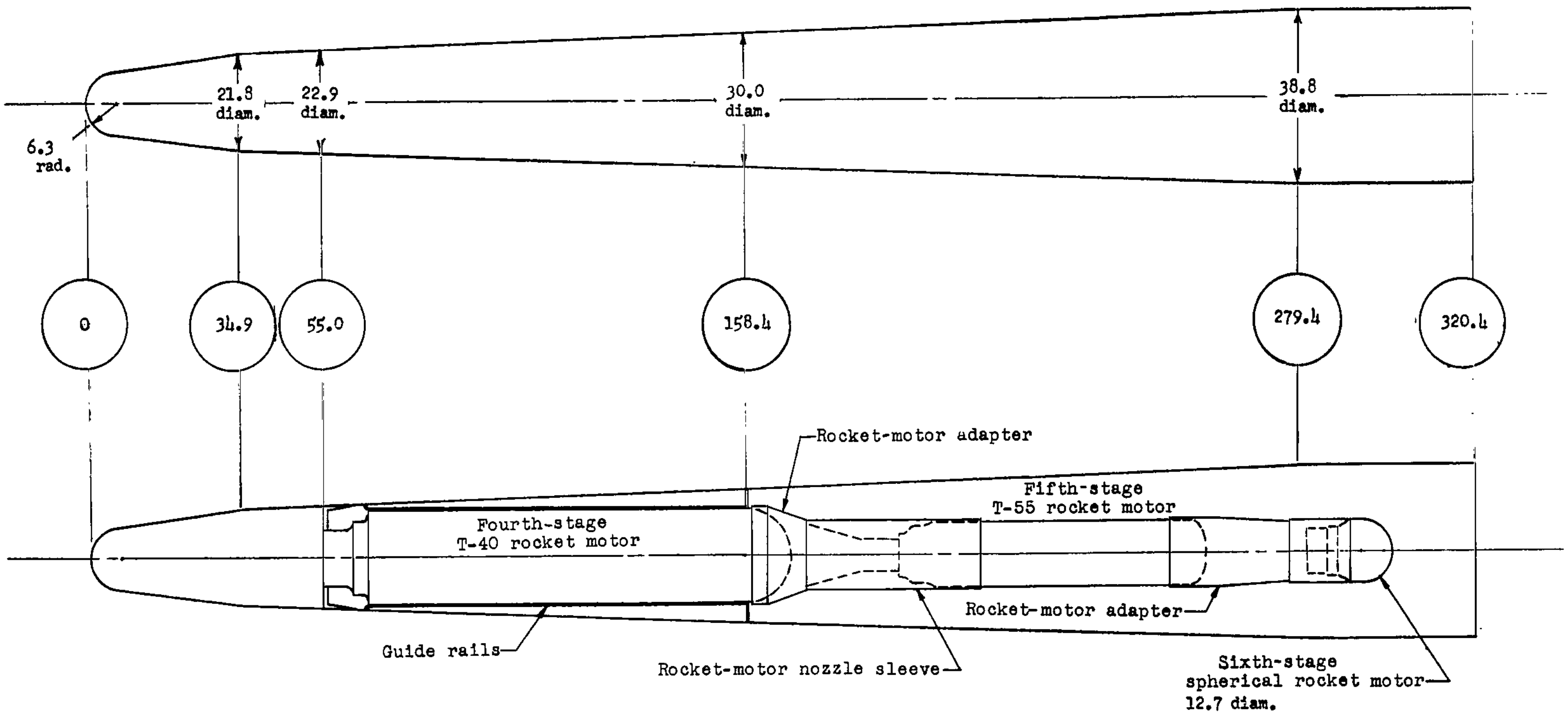

(a) Velocity package of six Trailblazer I vehicles with 12.7-centimeter-diameter reentry payloads.

Figure 3.- Typical sketch of velocity package. All dimensions and station locations are in centimeters.

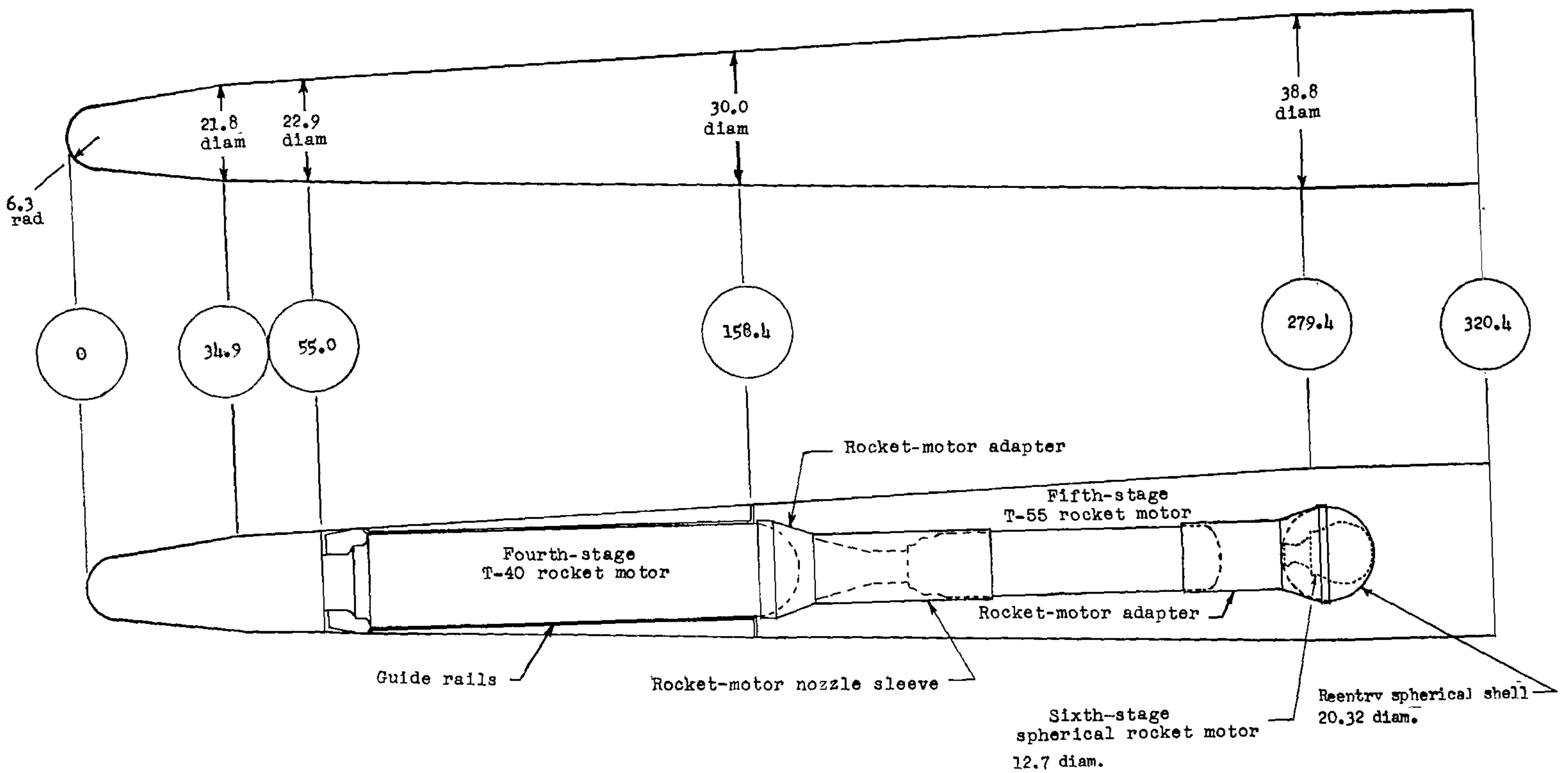

(b) Typical sketch of velocity package of two Trailblazer I vehicles with 20.32-centimeter-diameter reentry payloads.

Figure 3.- Concluded.

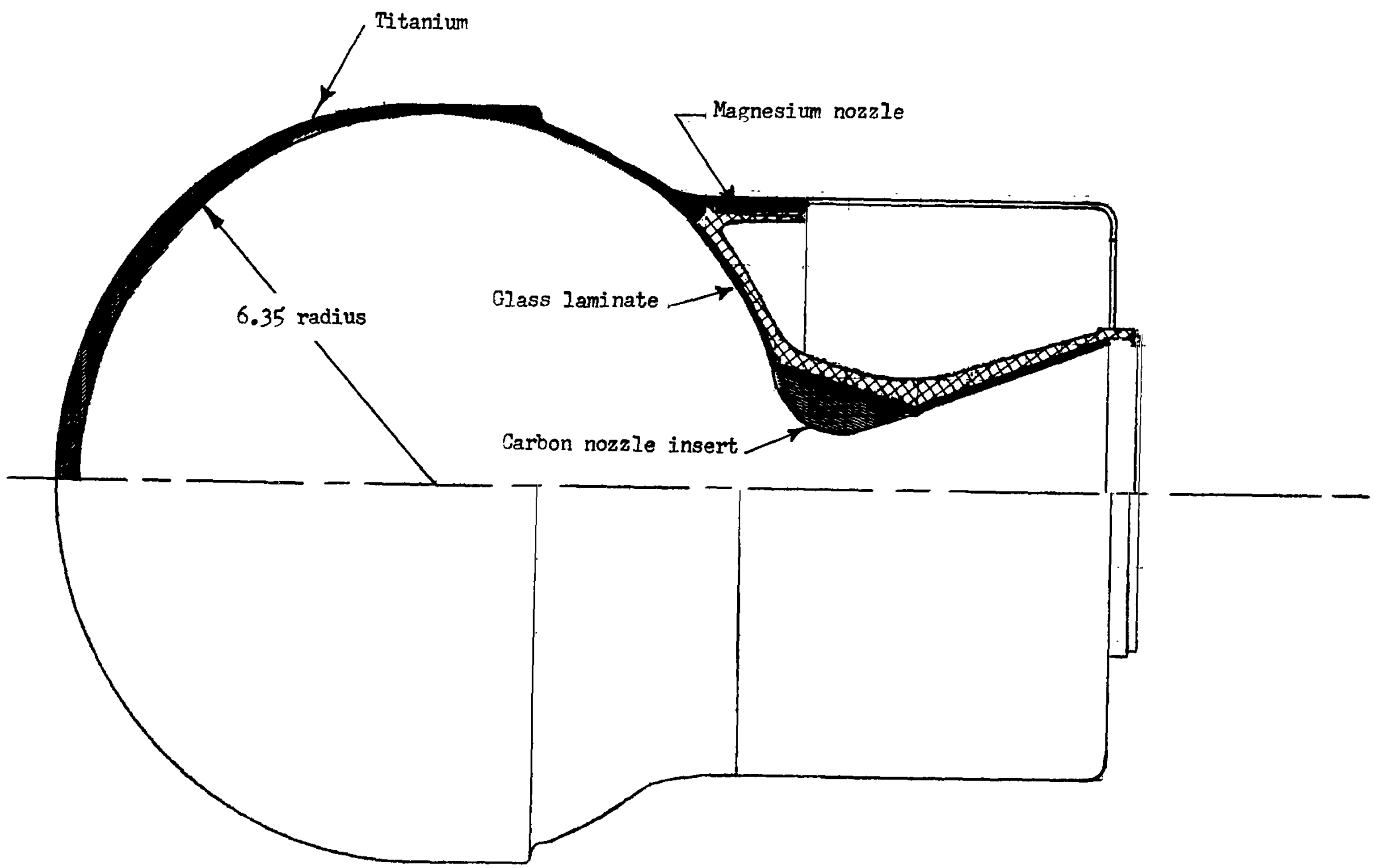

(a) Trailblazer Ic.

Figure 4.- Detail drawing of sixth-stage reentry bodies for eight Trailblazer I vehicles. All dimensions are in centimeters.

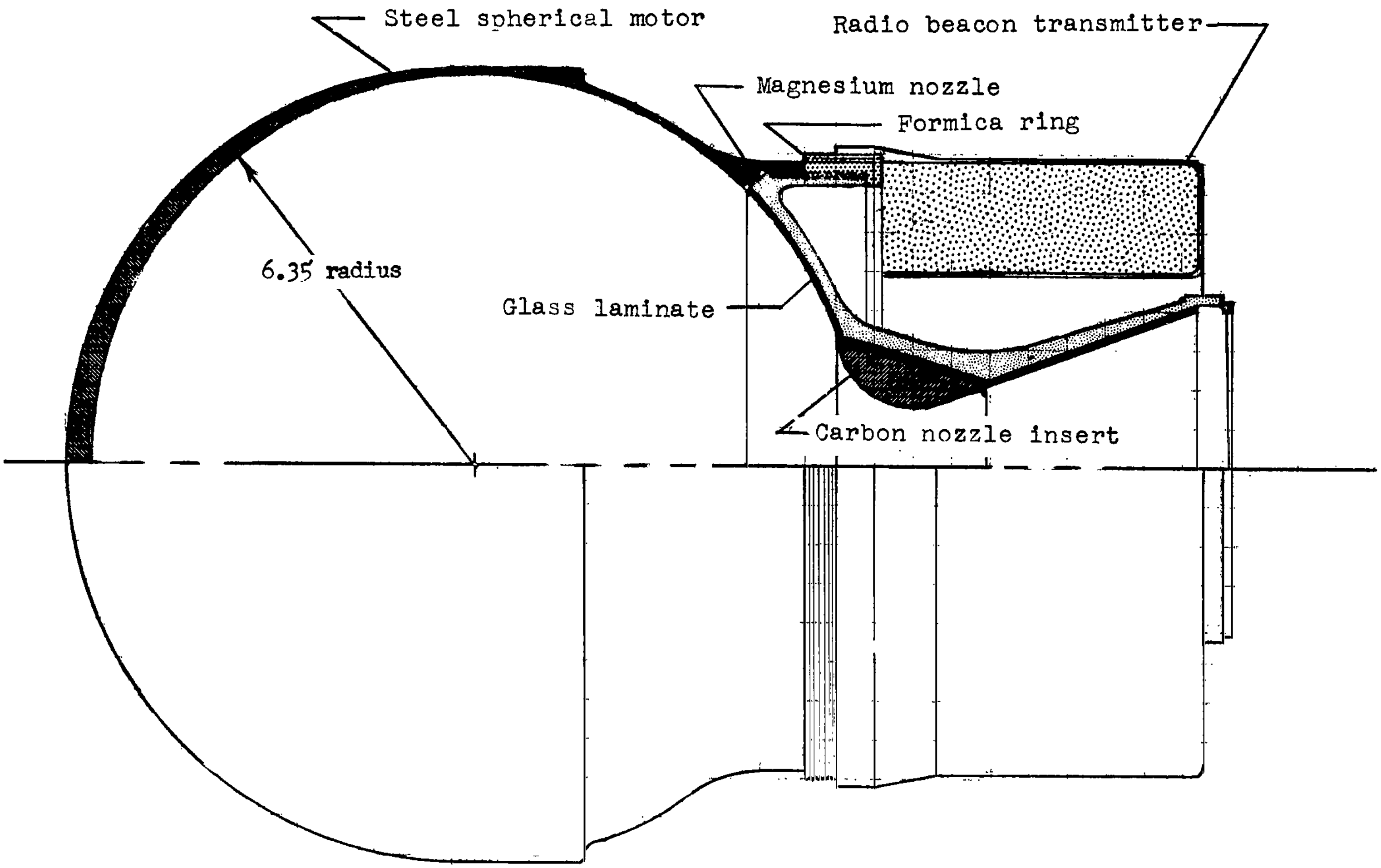

(b) Trailblazer Ie.

Figure 4.- Continued.

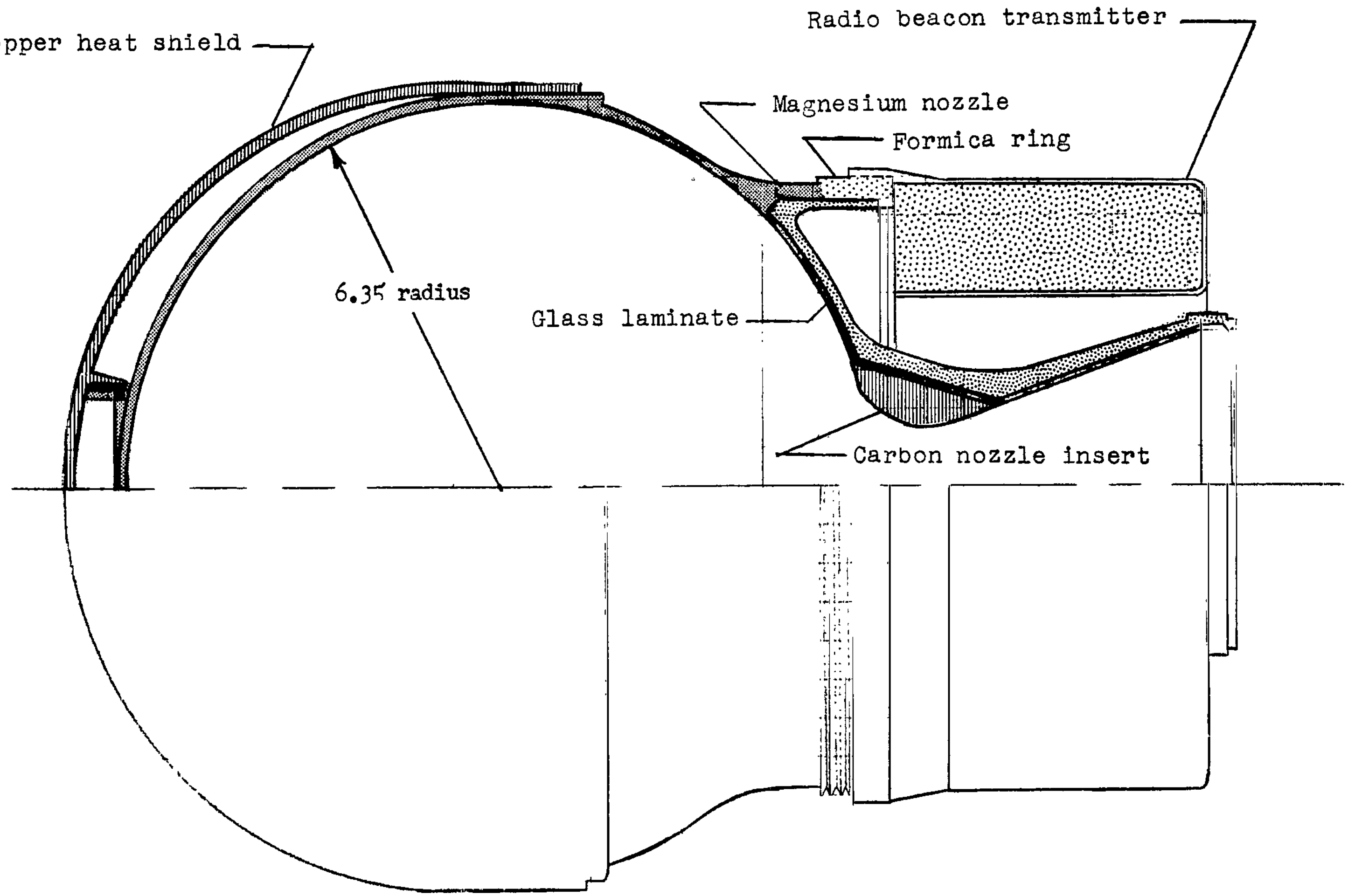

(c) Trailblazer If.

Figure 4.- Continued.

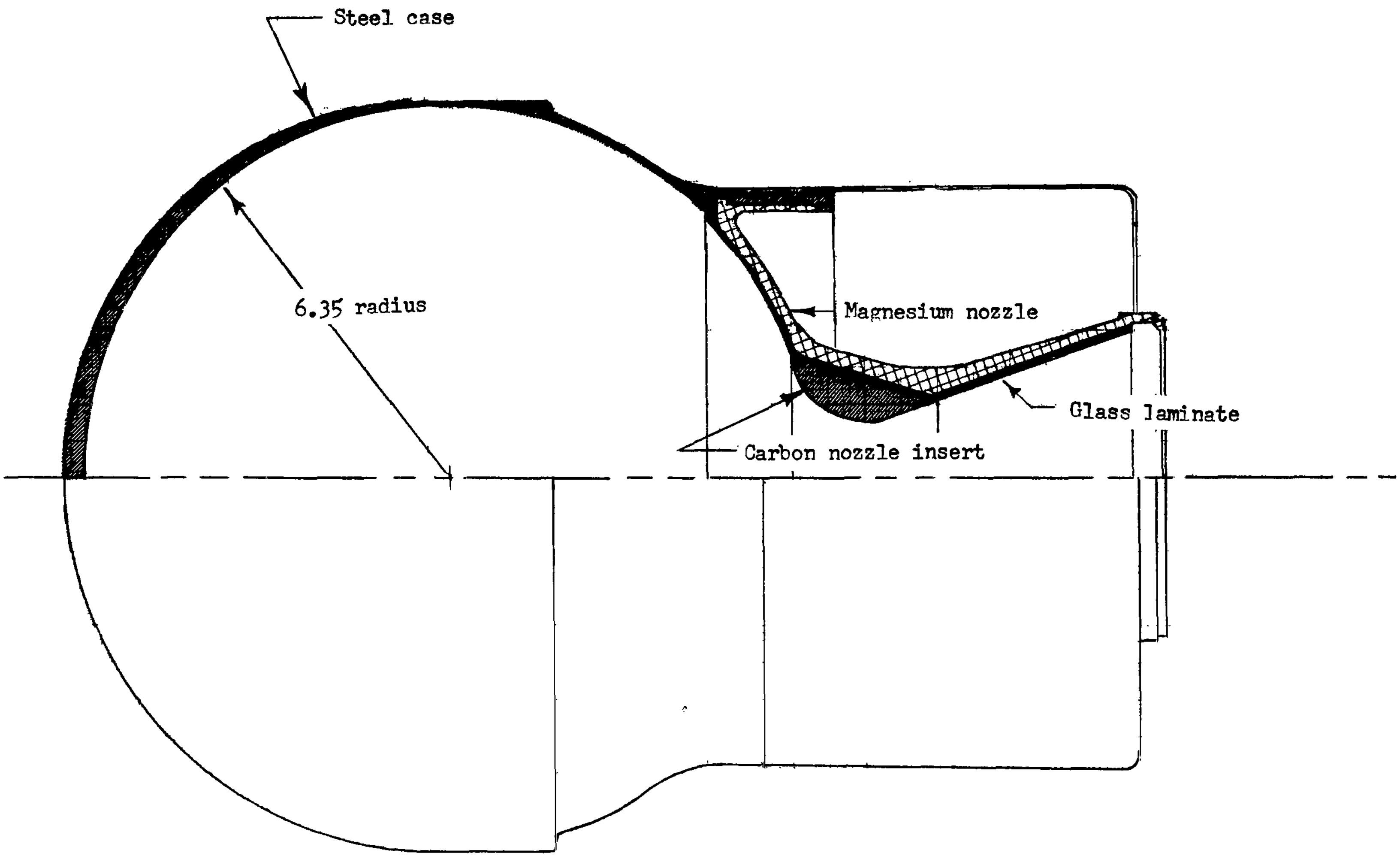

(d) Trailblazer Ih.

Figure 4.- Continued.

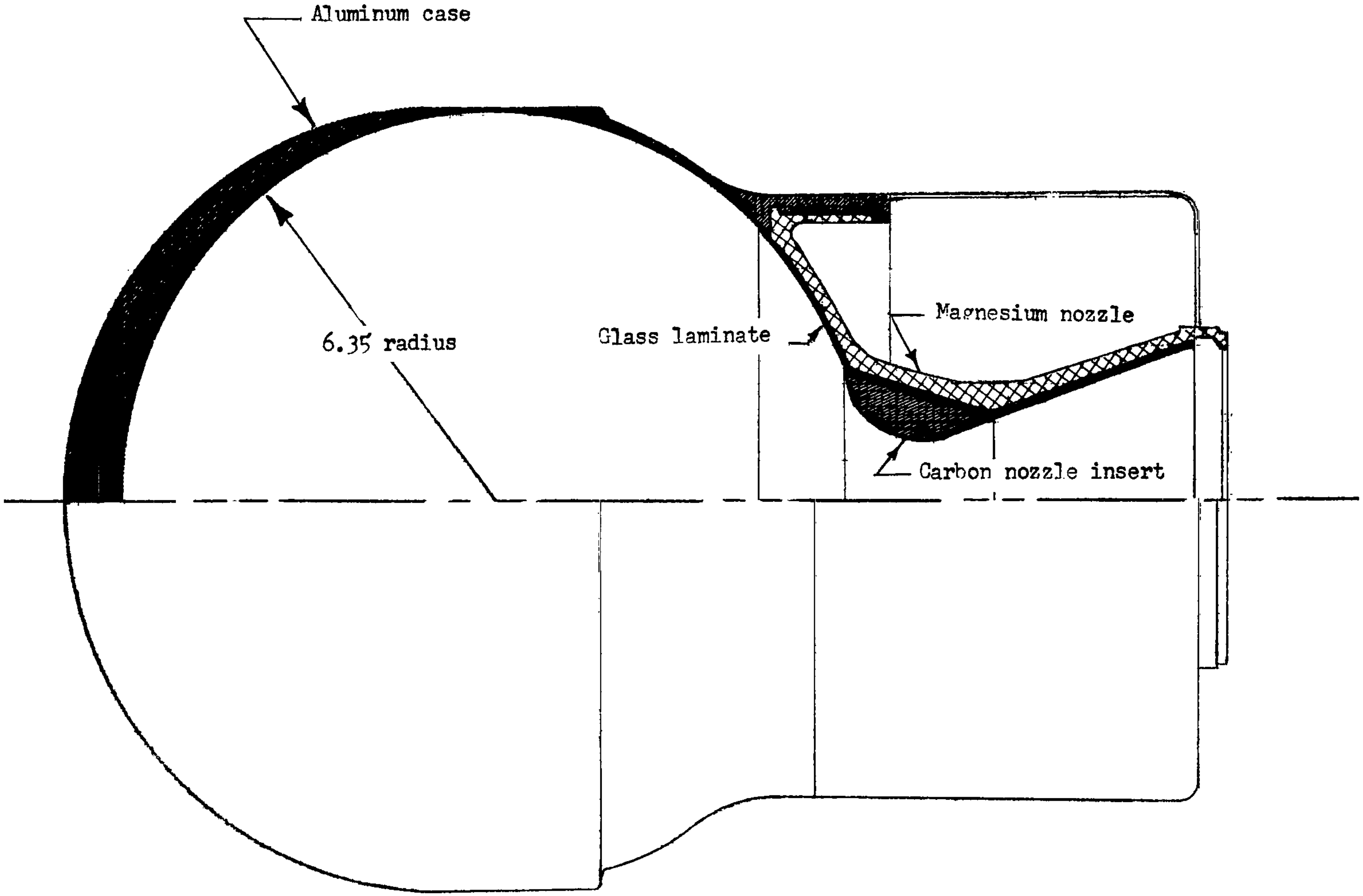

(e) Trailblazer Ii.

Figure 4.- Continued.

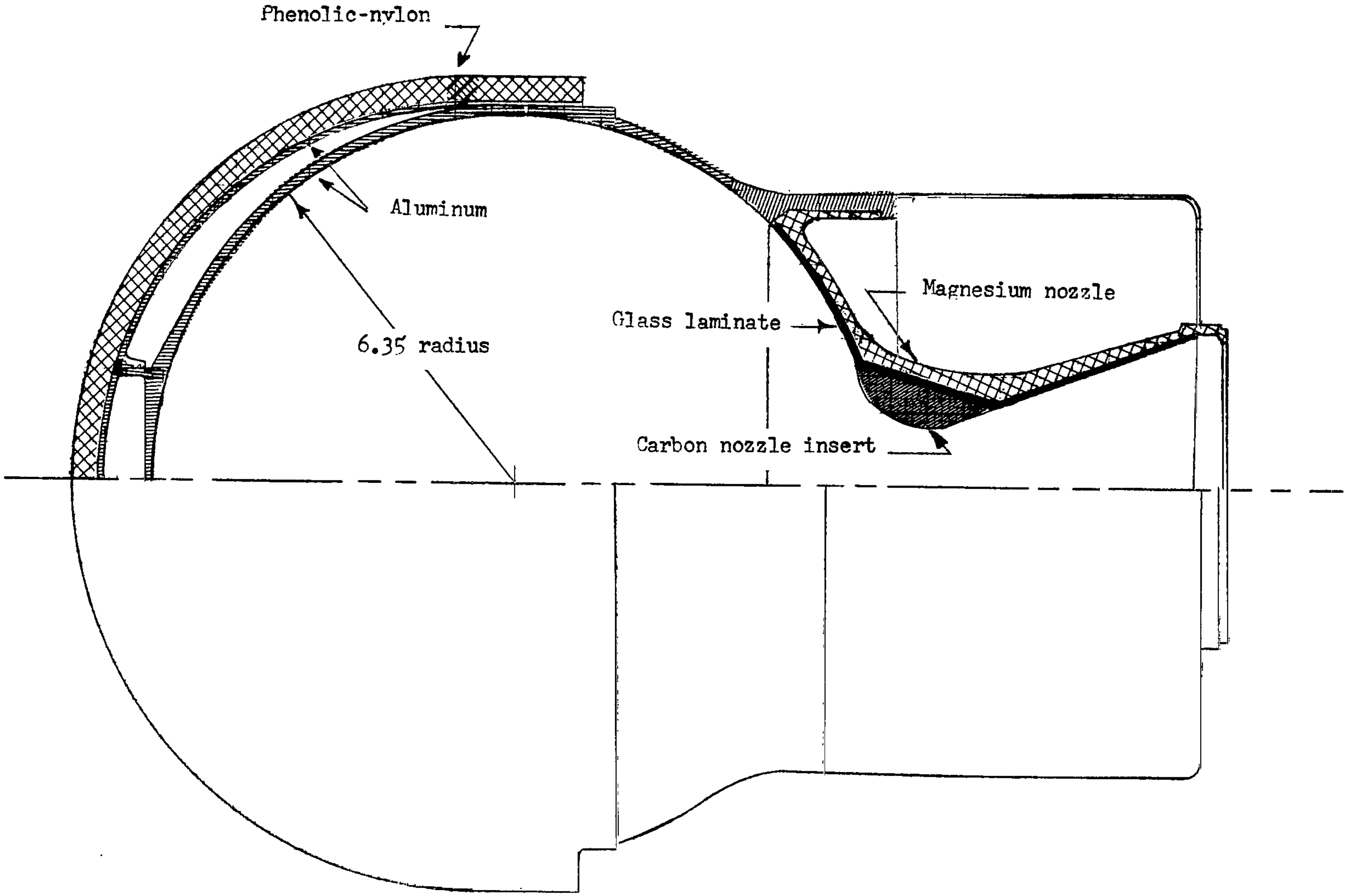

(f) Trailblazer Ij.

Figure 4.- Continued.

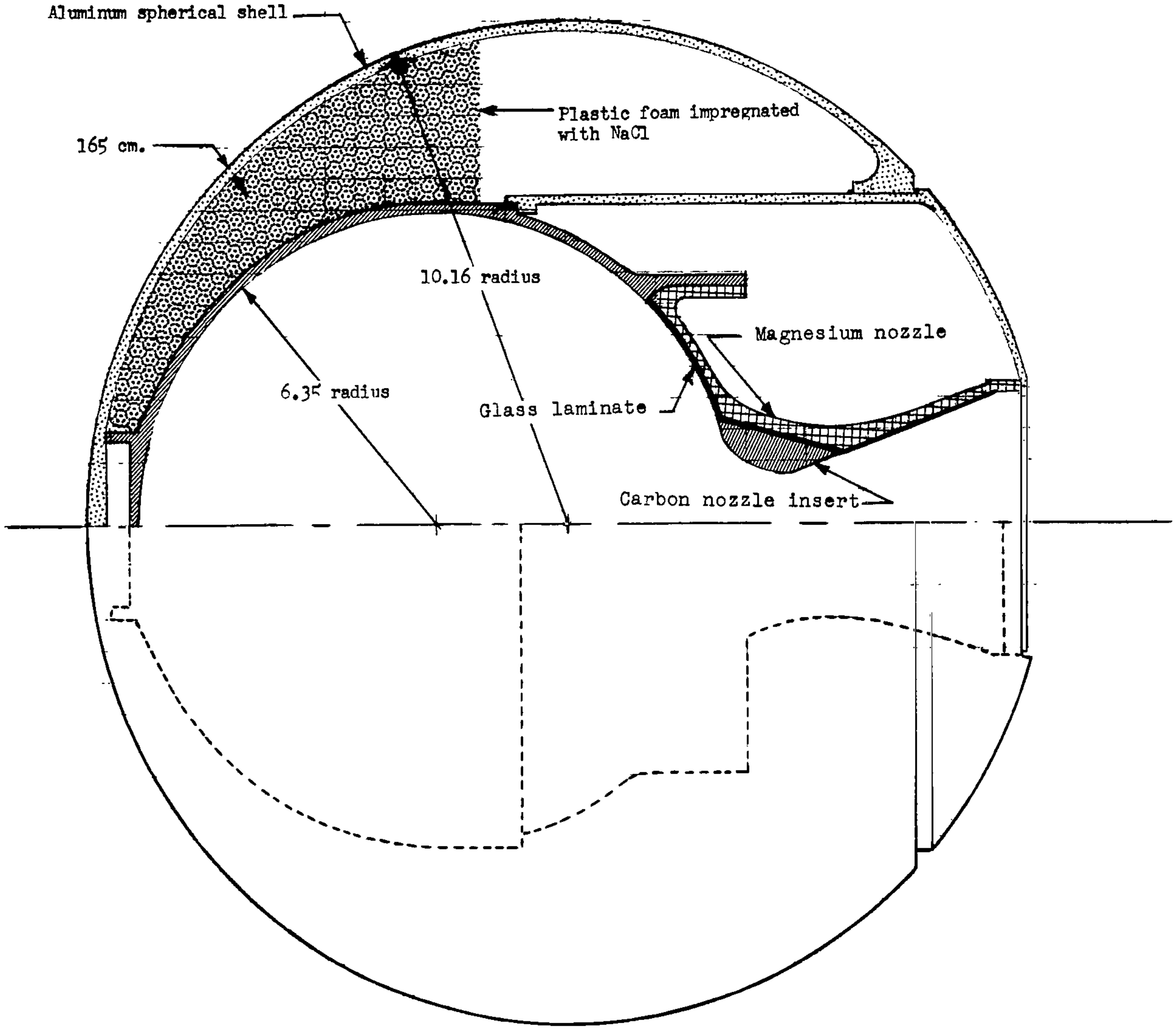

(g) Trailblazer Ik.

Figure 4.- Continued.

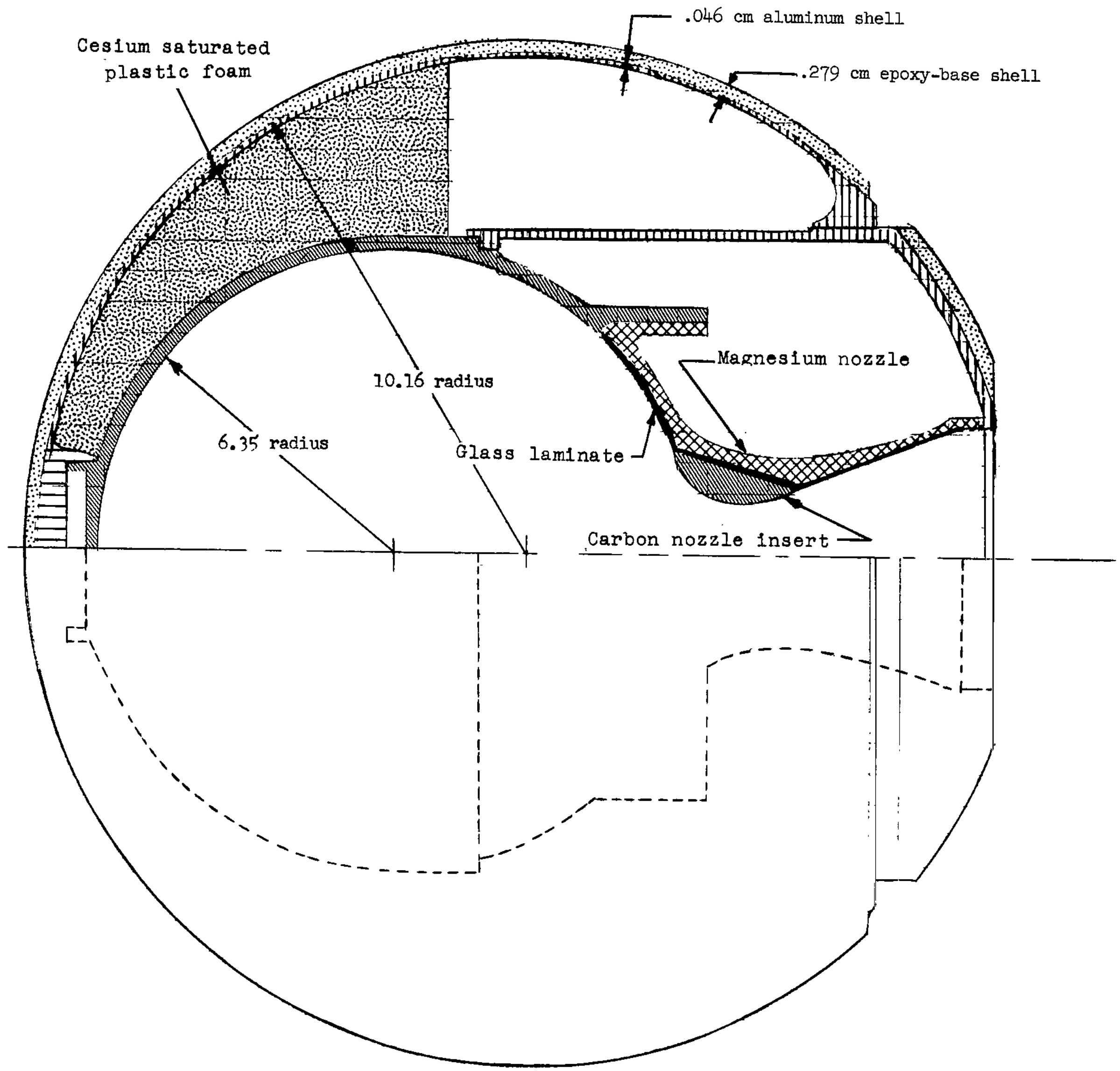

(h) Trailblazer Im.

Figure 4.- Concluded.

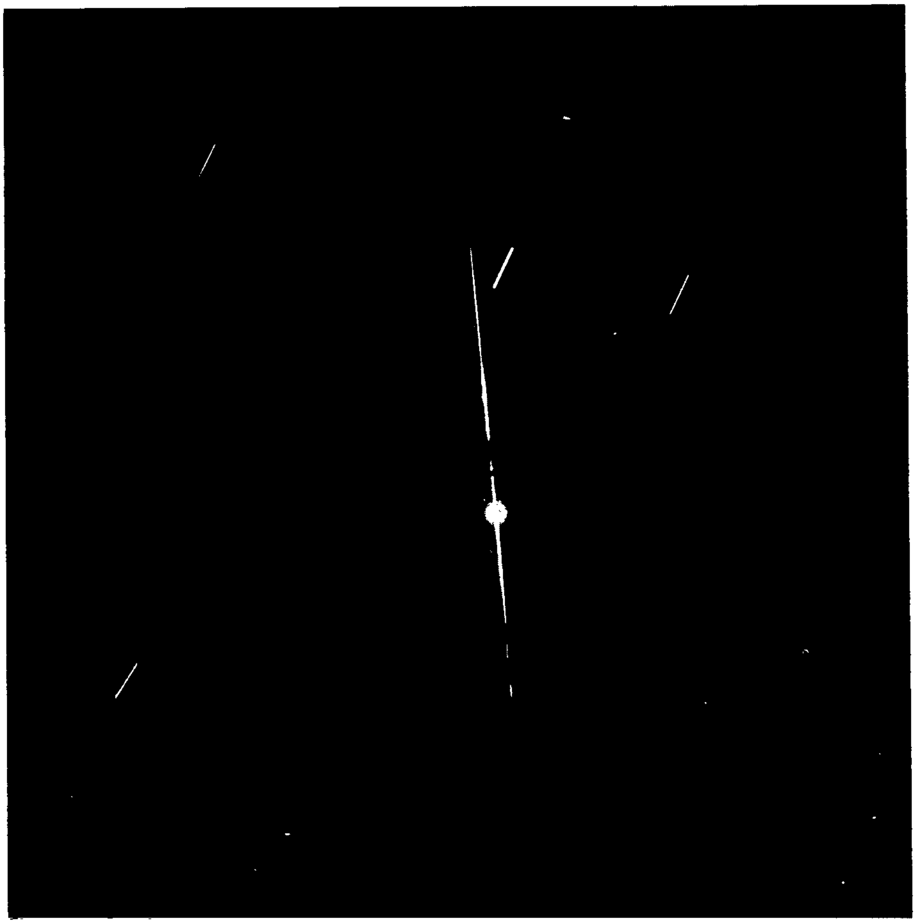

(a) Trailblazer Ic. L-63-9259

Figure 5.- Photographs of reentry streak of eight Trailblazer I vehicles.

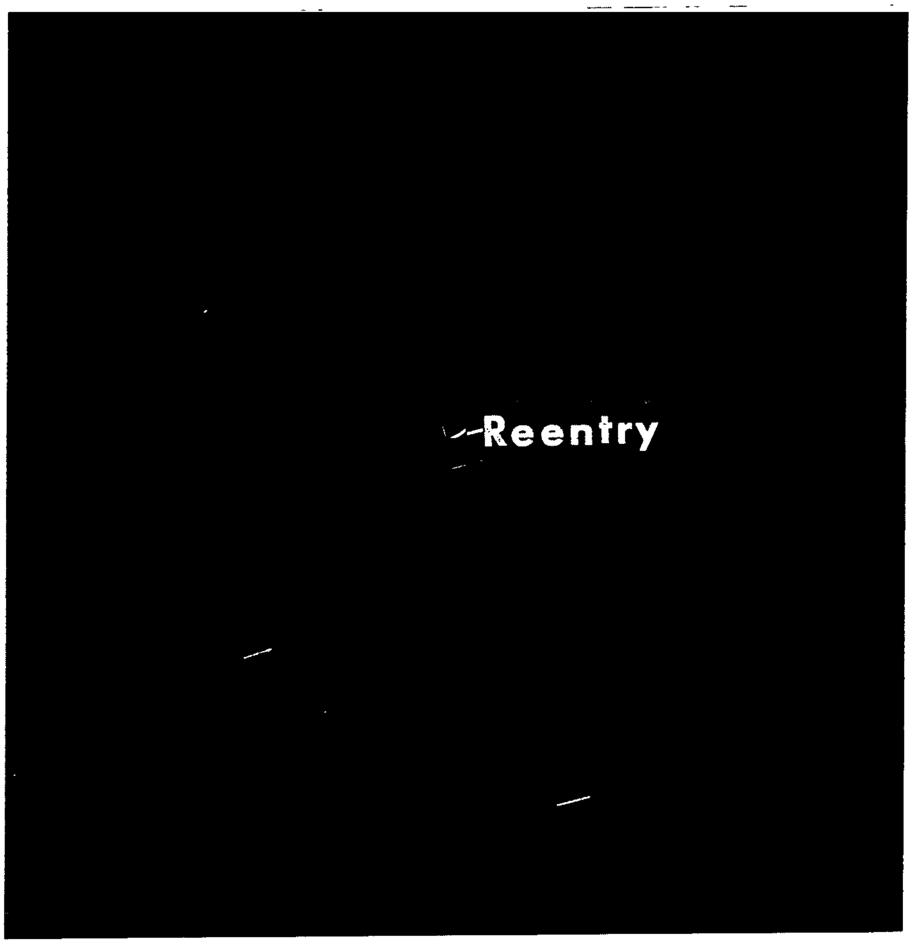

(b) Trailblazer Ie. L-63-9262

Figure 5.- Continued.

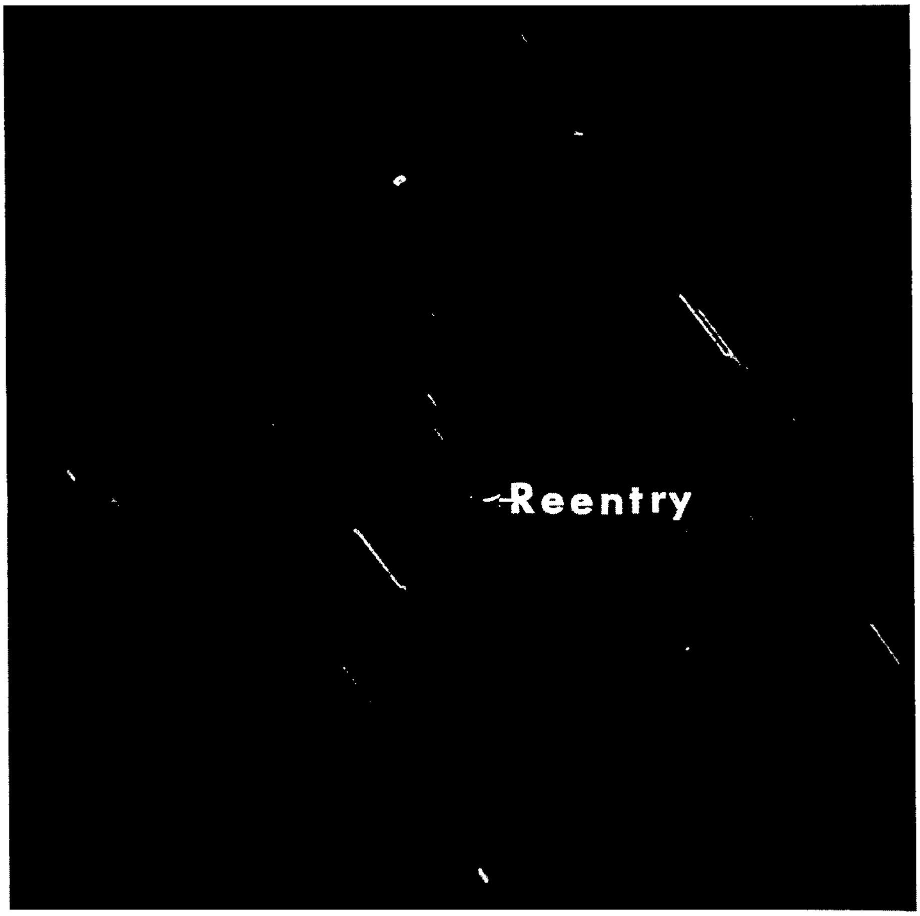

(c) Trailblazer If. L-63-9265

Figure 5.- Continued.

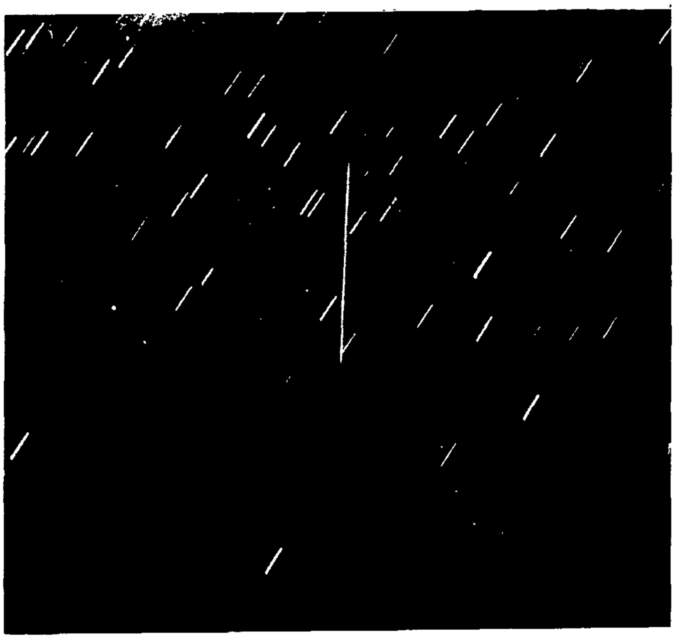

(d) Trailblazer Ih. L-66-4554

Figure 5.- Continued.

(e) Trailblazer II. L-65-7969

Figure 5.- Continued.

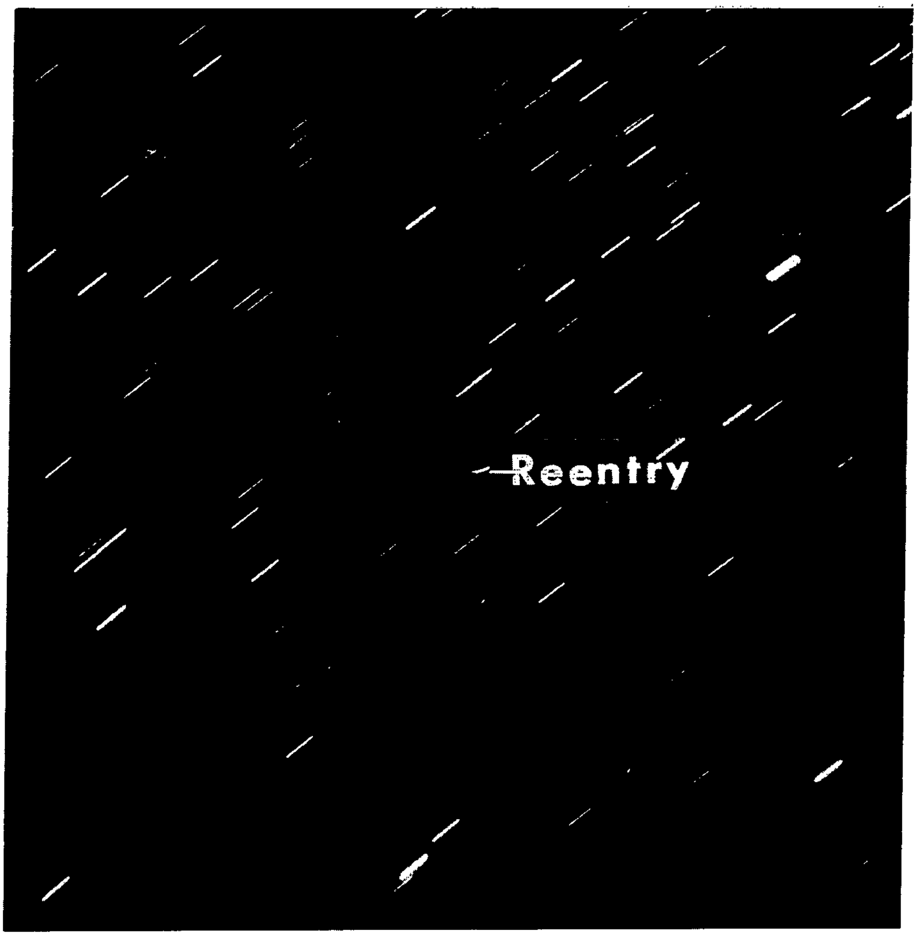

(f) Trailblazer Ij. L-66-4555

Figure 5.- Continued.

(g) Trailblazer Ik. L-66-4556

Figure 5.- Continued.

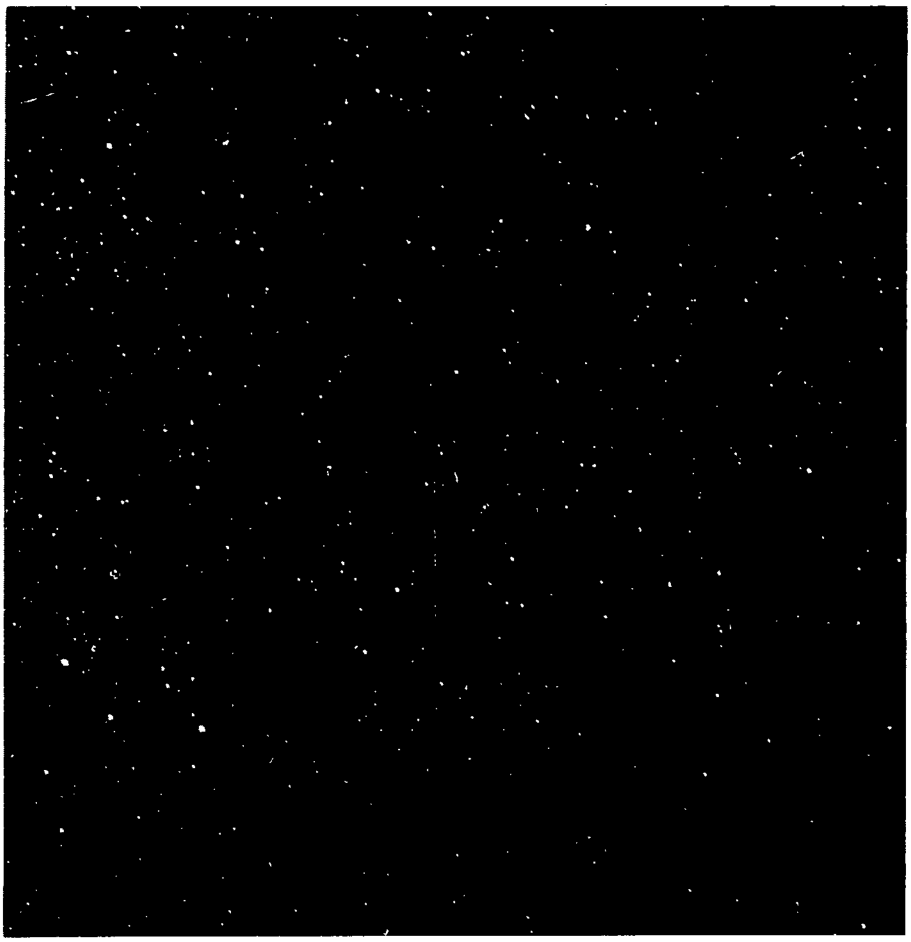

(h) Trailblazer Im. L-66-4557

Figure 5.- Concluded.

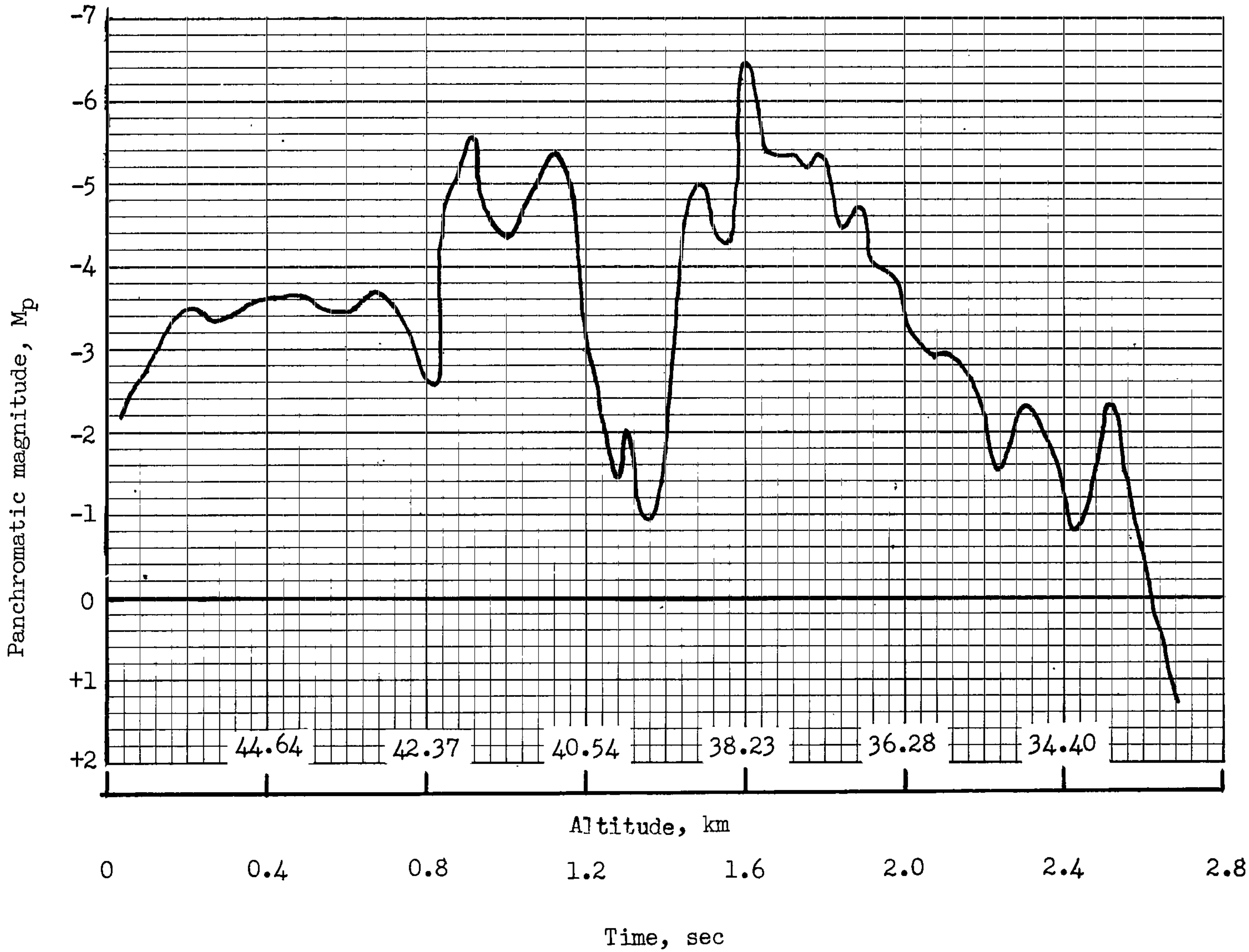

(a) Trailblazer Ic (titanium) reentry.

Figure 6.- Light curves for various Trailblazer reentries.

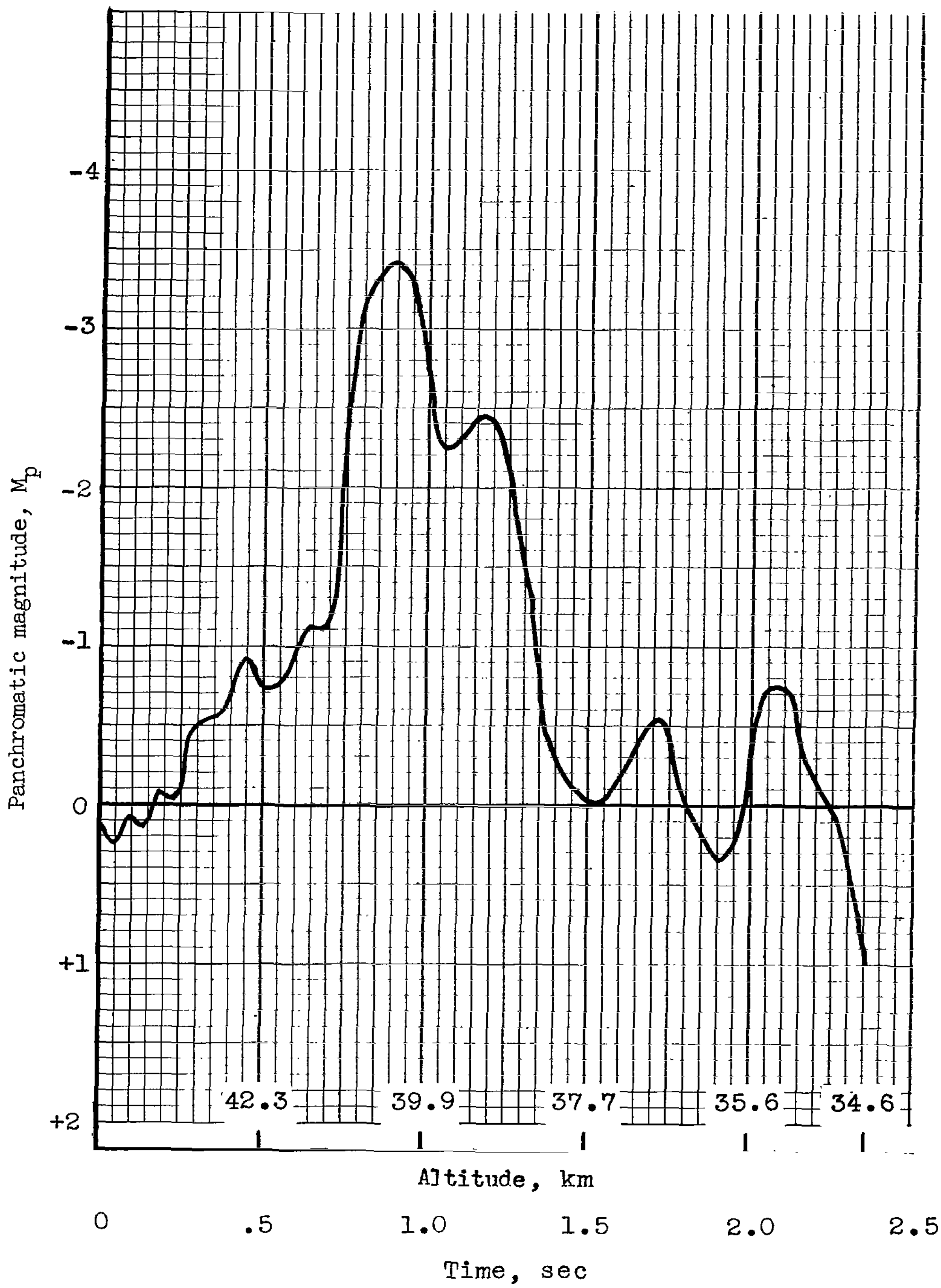

(b) Trailblazer Ie (steel) reentry.

Figure 6.- Continued.

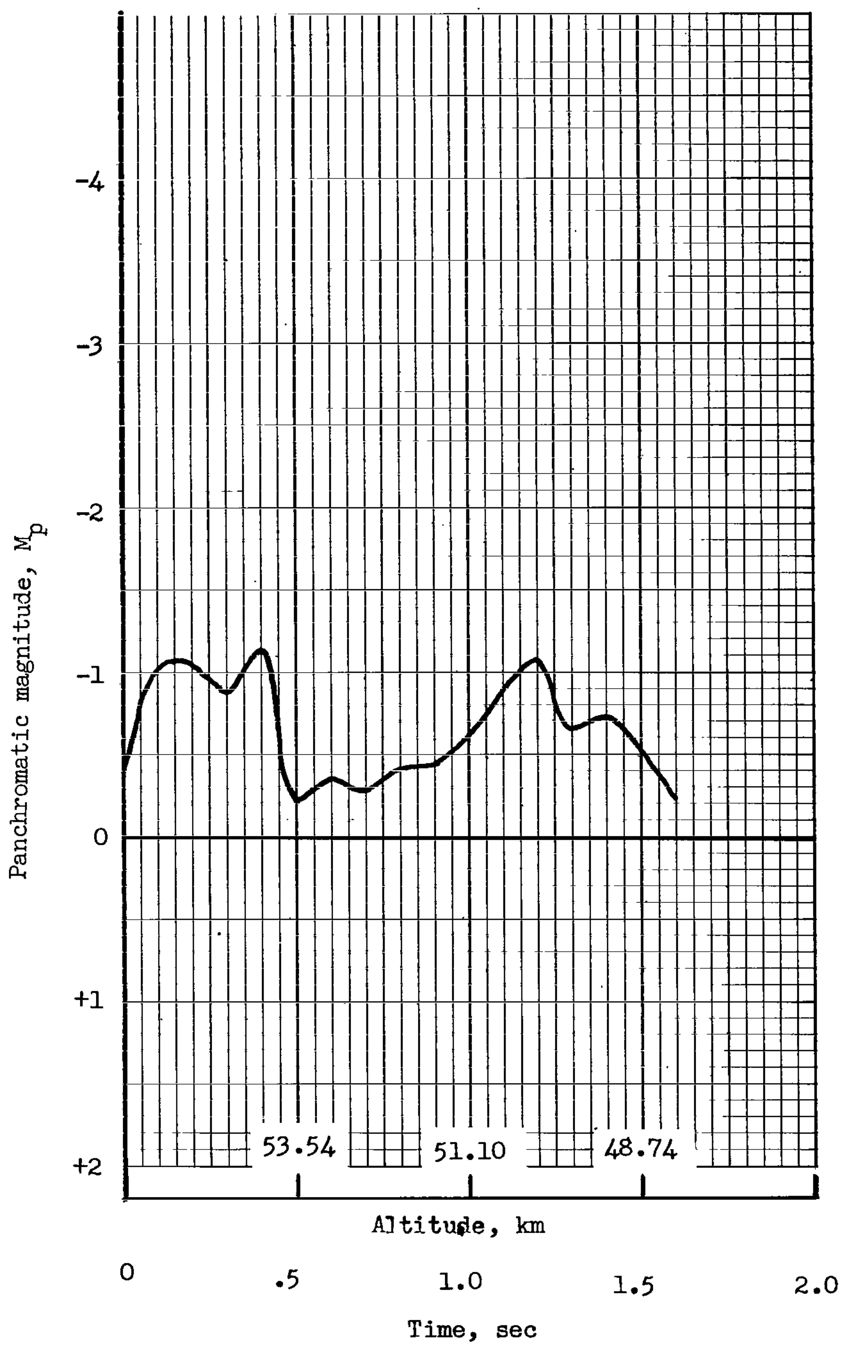

(c) Trailblazer IIf (aluminum with copper shield) reentry.

Figure 6.- Continued.

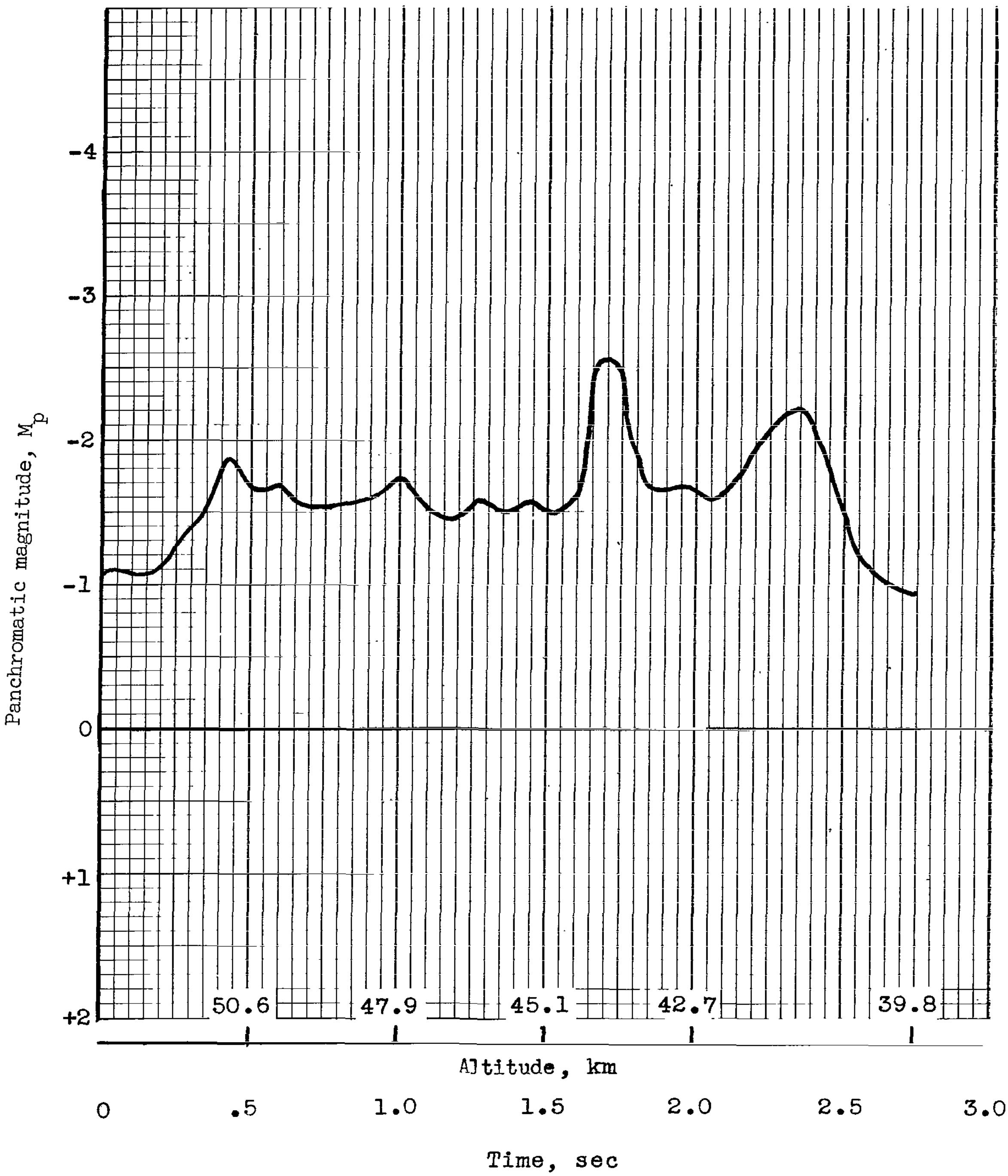

(d) Trailblazer Ih (steel) reentry.

Figure 6.- Continued.

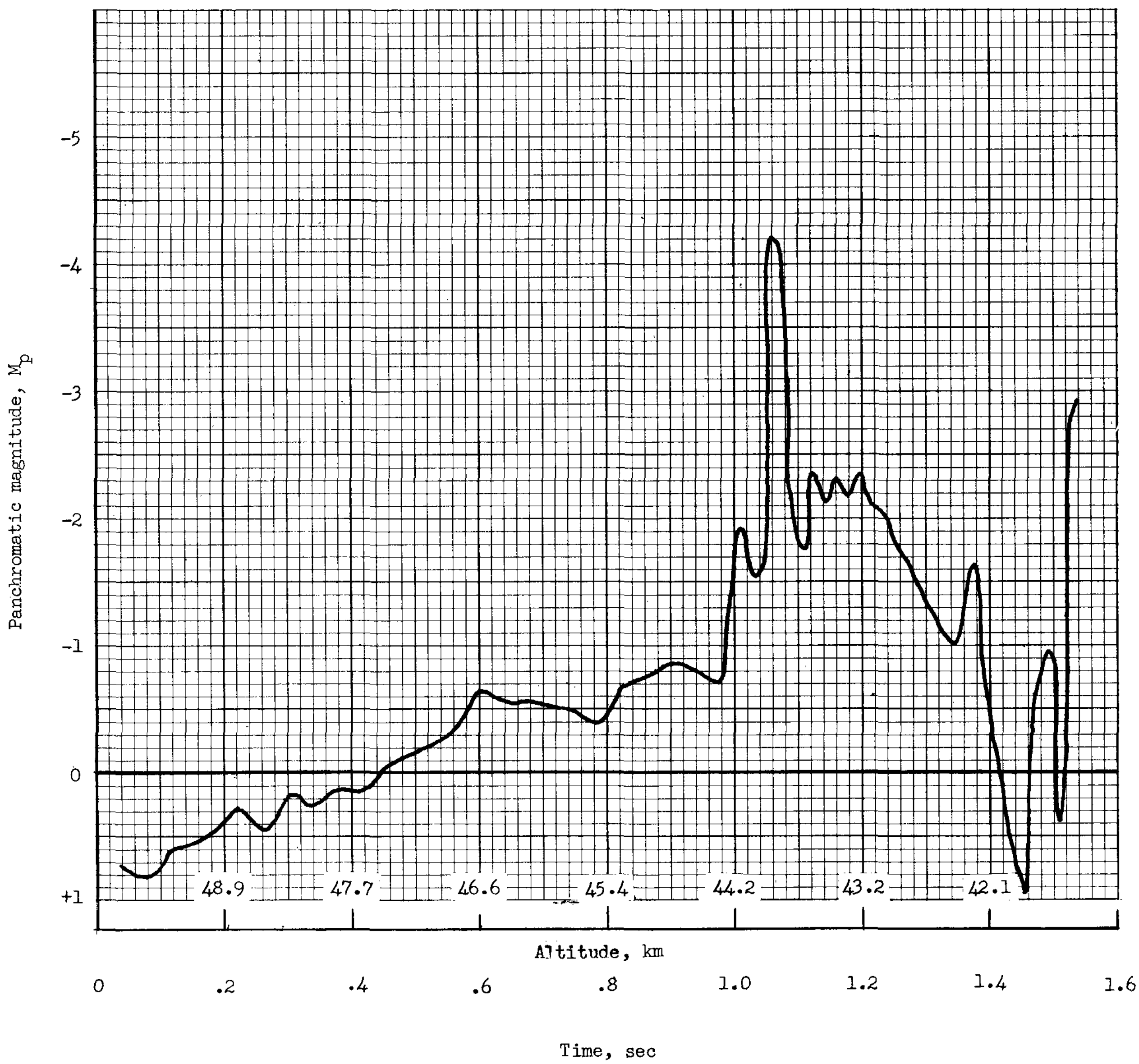

(e) Trailblazer II (aluminum) reentry.

Figure 6.- Continued.

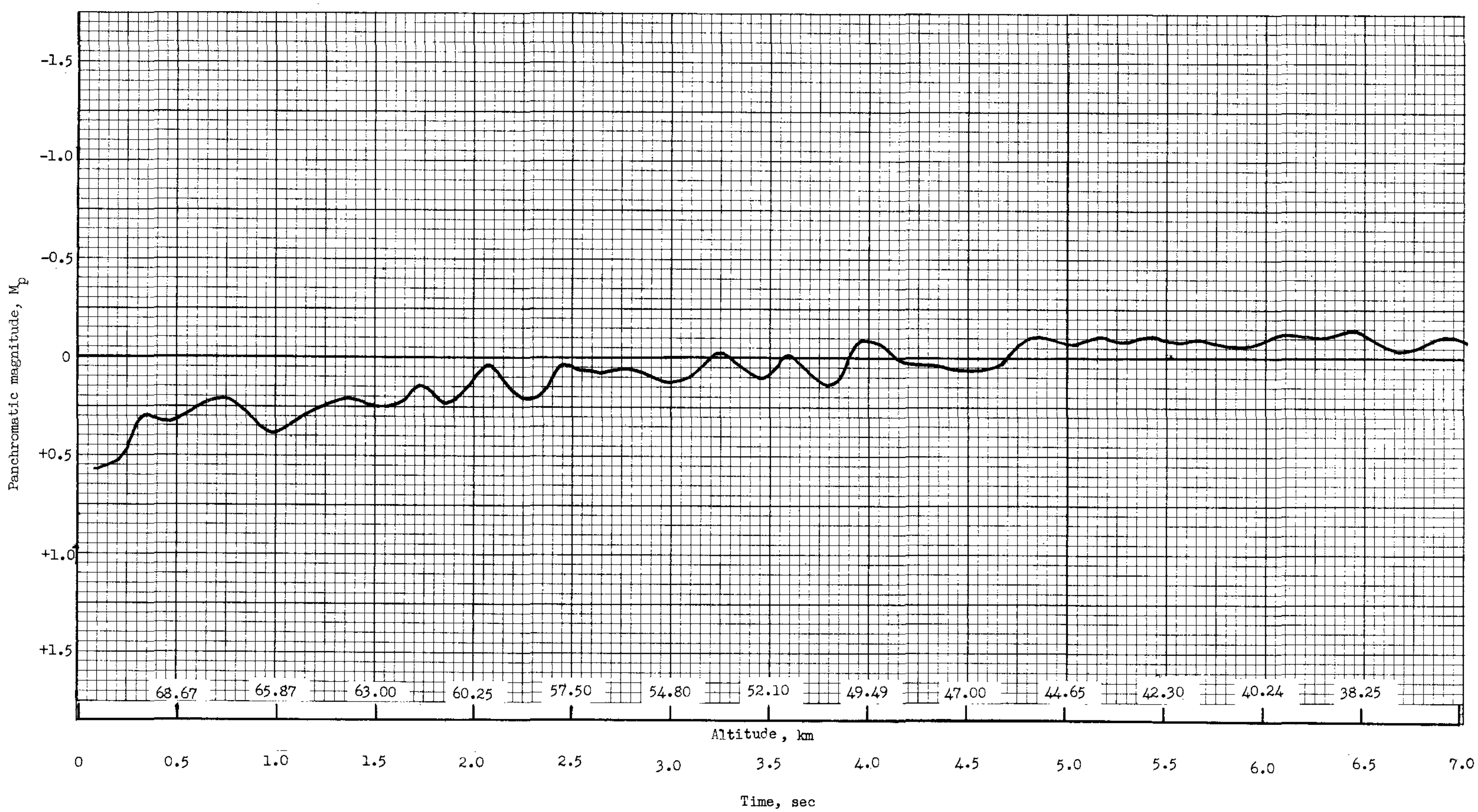

(f) Trailblazer Ij (phenolic-nylon) reentry.

Figure 6.- Continued.

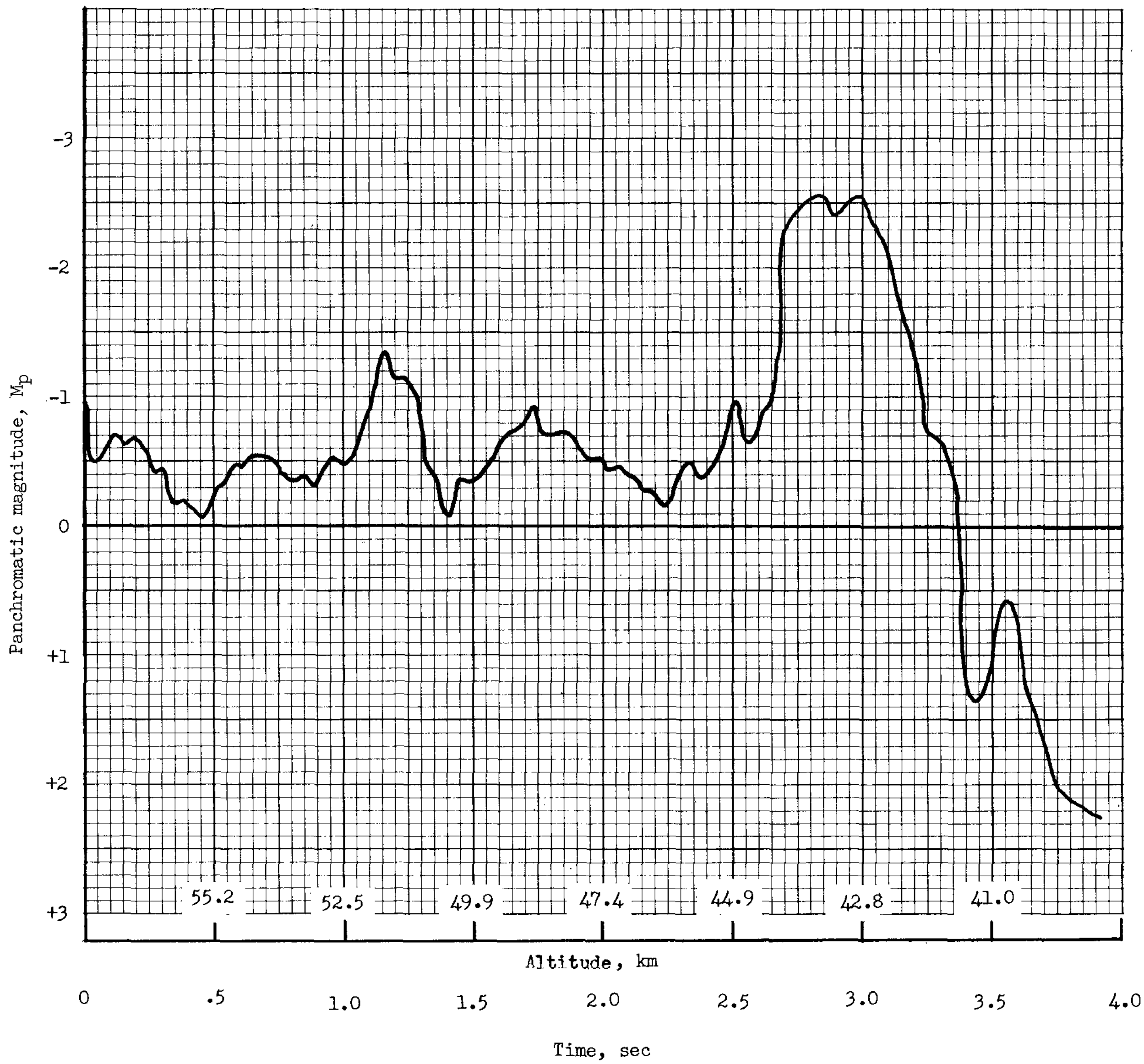

(g) Trailblazer Ik (20.32-cm-diameter aluminum sphere) reentry.

Figure 6.- Continued.

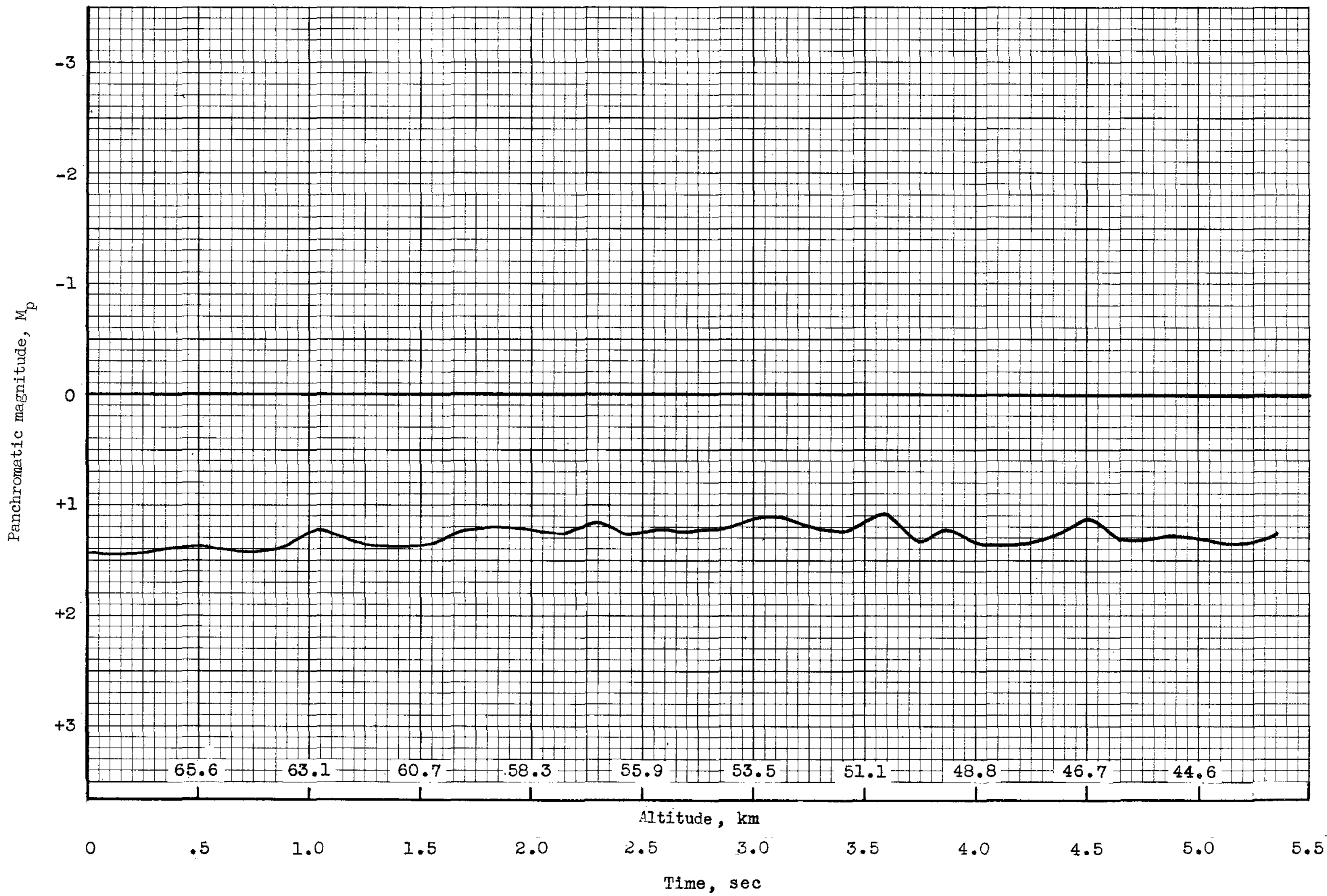

(h) Trailblazer Im (epoxy base) reentry.

Figure 6.- Concluded.

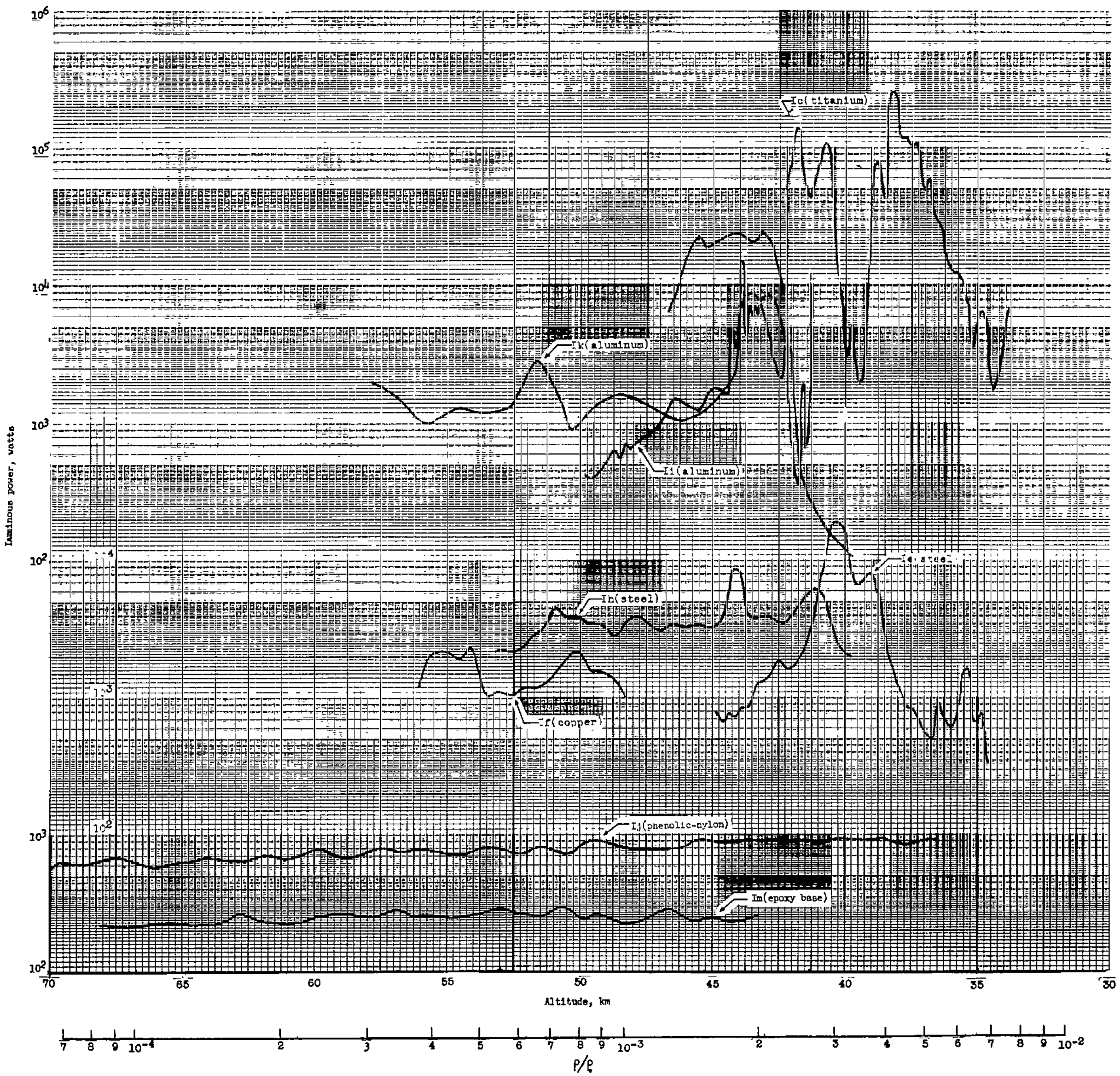

Figure 7.- Luminous energy as a function of height for eight Trailblazer I reentries.

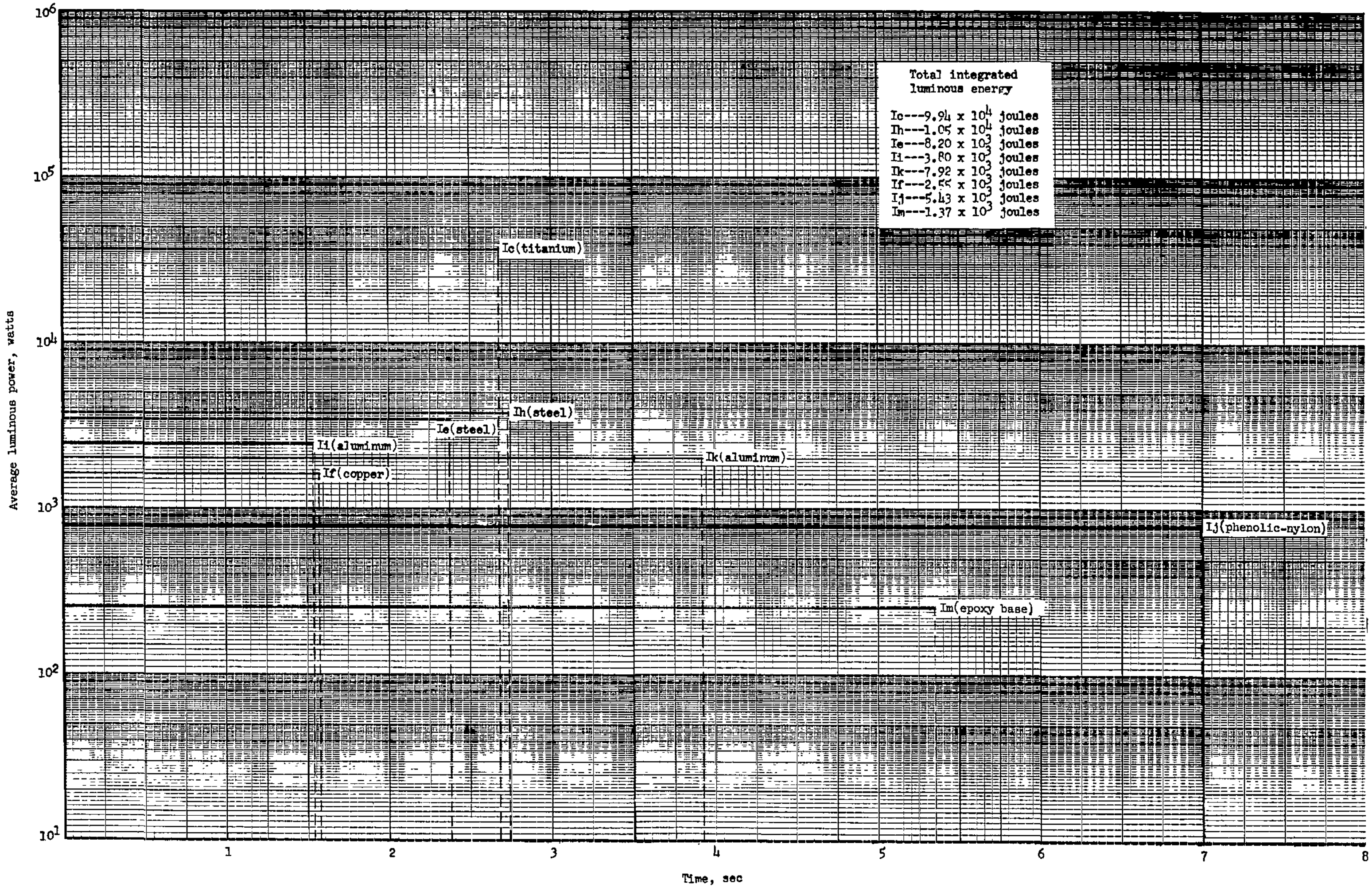

Figure 8.- Average luminous energy for eight Trailblazer I reentries.

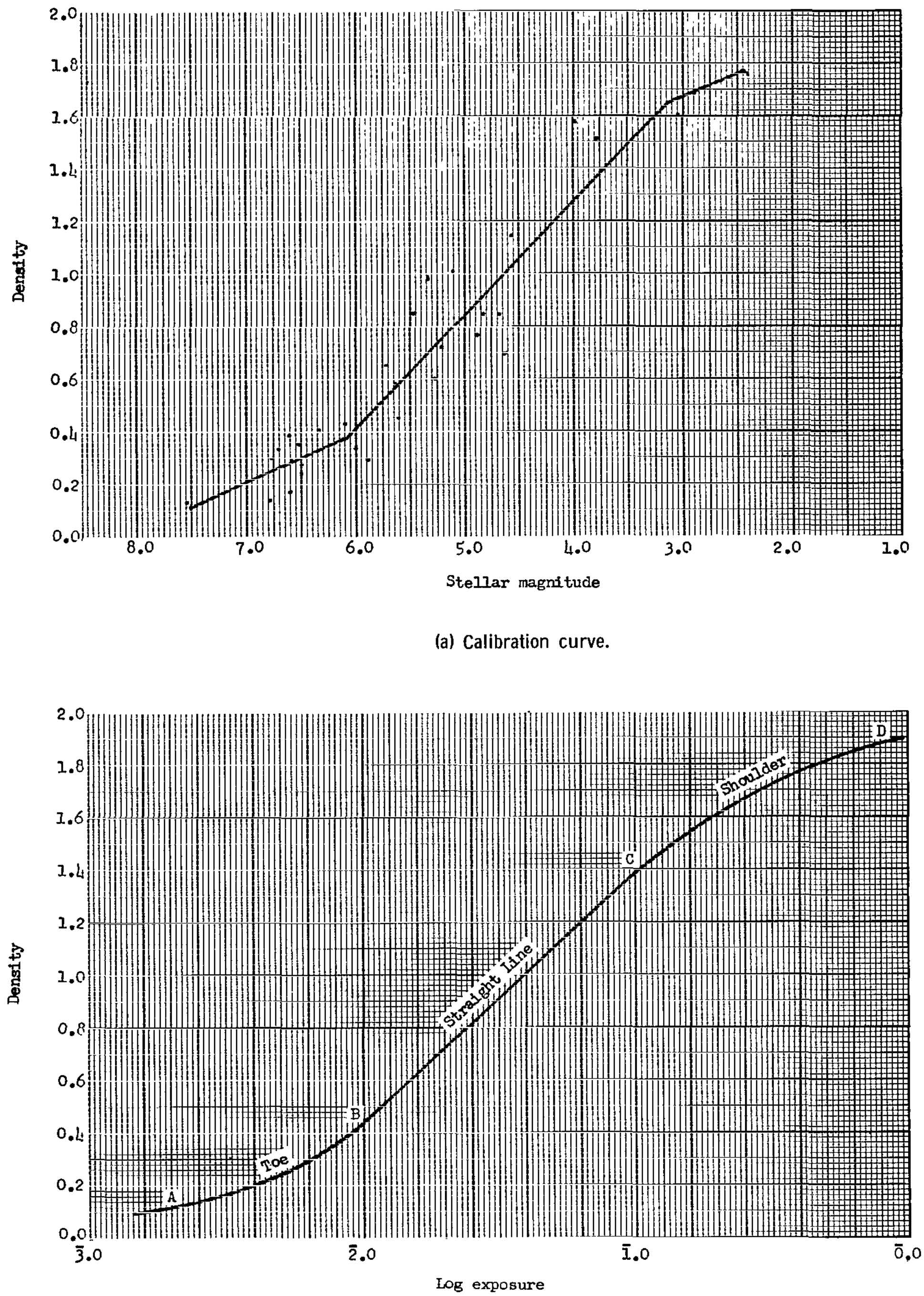

(a) Calibration curve.

(b) Characteristic H and D curve.

Figure 9.- Calibration curve and characteristic curve.

"The aeronautical and space activities of the United States shall be conducted so as to contribute . . . to the expansion of human knowledge of phenomena in the atmosphere and space. The Administration shall provide for the widest practicable and appropriate dissemination of information concerning its activities and the results thereof."

—NATIONAL AERONAUTICS AND SPACE ACT OF 1958

NASA SCIENTIFIC AND TECHNICAL PUBLICATIONS

TECHNICAL REPORTS: Scientific and technical information considered important, complete, and a lasting contribution to existing knowledge.

TECHNICAL NOTES: Information less broad in scope but nevertheless of importance as a contribution to existing knowledge.

TECHNICAL MEMORANDUMS: Information receiving limited distribution because of preliminary data, security classification, or other reasons.

CONTRACTOR REPORTS: Technical information generated in connection with a NASA contract or grant and released under NASA auspices.

TECHNICAL TRANSLATIONS: Information published in a foreign language considered to merit NASA distribution in English.

TECHNICAL REPRINTS: Information derived from NASA activities and initially published in the form of journal articles.

SPECIAL PUBLICATIONS: Information derived from or of value to NASA activities but not necessarily reporting the results of individual NASA-programmed scientific efforts. Publications include conference proceedings, monographs, data compilations, handbooks, sourcebooks, and special bibliographies.

Details on the availability of these publications may be obtained from:

SCIENTIFIC AND TECHNICAL INFORMATION DIVISION

NATIONAL AERONAUTICS AND SPACE ADMINISTRATION

Washington, D.C. 20546